NUCLEATION AND MORPHOLOGY OF ETCH PITS IN IRON

FACTORS INFLUENCING THE NUCLEATION AND MORPHOLOGY OF

CRYSTALLOGRAPHIC TYPE ETCH PITS

IN PURE IRON

By

GEOFFREY MARTIN SPINK, B.TECH. (HONS.)

A Thesis

Submitted to the Faculty of Graduate Studies

in Partial Fulfilment of the Requirements

for the Degree

Master of Science

McMaster University

August 1969

MASTER OF SCIENCE (1969)   McMASTER UNIVERSITY
(Metallurgy)   Hamilton, Ontario.

TITLE: Factors influencing the Nucleation and
           Morphology of Crystallographic Type Etch
           Pits in Pure Iron.

AUTHOR: Geoffrey Martin Spink, B.Tech.(Hons)
                         (Brunel University)

SUPERVISOR: Professor M. B. Ives.

NUMBER OF PAGES: vii, 48

SCOPE AND CONTENTS: Etch pits can be produced in iron whose
                        shape reflects the crystallography of
                        the crystal. It is shown that pit
                        morphology can be adequately predicted
                        from an orientation dependent dissolution
                        theory. The influence of an air-formed
                        surface oxide film on pit nucleation and
                        morphology is demonstrated.

A C K N O W L E D G M E N T S

CONTENTS

(v)

LIST OF FIGURES

CHAPTER I

INTRODUCTION

The discovery that etch pits could be formed at the points of emergence of line defects at a crystal surface provided a major breakthrough in the search for experimental confirmation of the existence of dislocations.

By the early 1950's dislocation theory had reached a high state of perfection.(1) At a discussion on crystal growth organised by the Faraday Society in 1949(2) Frank pointed out that it was necessary to assume the presence of some crystal defect in order to explain the observed rates of growth of crystals under conditions of low supersaturation. He showed that the presence of a screw dislocation would eliminate the need for the formation of successive two dimensional nuclei during growth and concluded that its presence would be revealed by spiral terraces on the crystal surfaces.

Shortly after this discussion Griffin observed such spiral terraces on habit faces of beryl crystals, which was followed by similar observations by Verma(3) and Amelinck(4) on carborundum crystals and by Dawson and Vand on paraffins(5). The first dynamic observations of the operation of screw dislocation mechanisms were made by Forty who studied the growth of cadmium iodide crystals from solution(6).

A start had been made in the experimental verification of the presence of dislocations but these early observations of surface topography were severely limited in that only screw dislocations (those with a component of the Burgers vector normal to the surface) could be detected and then only on naturally occurring habit faces or cleavage surfaces.

Again it was Frank who pointed out(2) that dissolution on a crystal habit face should proceed in a manner closely equivalent to growth by unbuilding terraces ending at screw dislocations. This was verified by Horn(7) who etched silicon carbide crystals in fused sodium carbonate at 1,000°C.

It was the classical work of Vogel et al(8) in 1953, however, which provided the evidence needed to stimulate research and firmly establish the etch pitting technique as a reliable method of detecting dislocations at a free surface.

They developed an etching technique which produced conical pits on {100} and {110} faces of germanium single crystals. The pits were evenly spaced in rows and were thought to correspond to dislocations in a simple tilt boundary predicted by theory. The angle of tilt was measured by X-ray methods and the linear density of dislocations expected from the theory calculated. This value was found to agree with the observed linear density of etch pits. In this case, then, edge dislocations had been revealed by an etch pit method.

Following this work, Vogel(9) showed that pits formed aligned in slip traces in germanium single crystals. He demonstrated glide polygonisation due to deformation at high temperature and polygonisation produced by annealing after deformation.

Dash(10) decorated dislocations in silicon by the precipitation of copper and developed pits on faces of all orientations.

Gilman and Johnson(11) demonstrated the continuity of line defects by etching the two mirror halves of a cleaved surface of lithium fluoride.

They demonstrated the introduction of fresh dislocations after plastic deformation and distinguished between edge and screw orientations.

The etch pit method is thus extremely useful for firstly detecting dislocations at free surfaces and secondly for tracing their movements. The processes of slip, glide polygonisation, annealing polygonisation and dislocation multiplication can be followed in detail. Normally, however, only certain orientations are etched and it is not always easy to establish a definite one-to-one correspondence between pits and dislocations. Entirely satisfactory results are usually only obtained with single crystals having low dislocation densities and easily cleaved low index faces. In etching polycrystalline metals, for example, dislocation densities are so high that pits often overlap giving an overall surface etch in which individual pits cannot be distinguished.

The rate of two dimensional nucleation at a dislocation depends upon the details of its core and the depth of pits in a given crystal may therefore vary. In lithium fluoride, for example, deeper pits are formed at edge dislocations than at screw, and dislocations at which certain impurities have segregated produce shallower pits than do clean ones.

Most investigations studying the etching of metals have found that an aging treatment is necessary in order to "decorate" the dislocations with an impurity segregate. It is possible that the impurity enhances the rate of attack at the line defect which would otherwise have such a low chemical potential as to render pit growth unlikely. Impurity atoms will tend to segregate towards the distorted area of an edge dislocation and may accumulate in such quantity as to form a precipitate.

Suits and Low(12) have shown that aging is necessary for etch pitting of dislocations in a Fe-3% Si alloy and that carbon is the principal segregating impurity.

Pickering(13), working with polycrystalline Fe-3% Si iron, found that a one-to-one correspondence between etch pits and dislocations is only possible when the dislocation density is below a critical value which cannot be displaced upwards by increasing the carbon content. Direct observation of pitted areas in etched thin foils was made under the electron microscope. Fresh dislocations introduced by plastic deformation were never pitted whereas aged dislocations were nearly always attacked. Pickering concluded that for a one-to-one correspondence to exist the amount of carbon in solution must be (a) equal to, or above, that level which is necessary to produce sufficiently large carbon atmospheres at every dislocation present in the alloy during aging; and (b) below that level which, by the formation of random clusters or precipitates during aging, is sufficient to cause two-dimensional nucleation of etch pits not associated with dislocations.

Hibbard and Dunn(14), also working on silicon iron, obtained good agreement between observed and calculated dislocation densities for $\langle 112 \rangle$ edge dislocations in bent single crystals. They observed cancellation of unlike dislocations during removal of a polygonisation structure and of a cold worked structure, and the change in distribution of dislocations after bending and annealing.

The etching technique developed by Livingston(15) distinguishes between positive and negative edge dislocations on the $\{111\}$ surfaces of copper single crystals. Observations on bent crystals show that 95% of the dislocations are of the majority sign, implying that most of them were

generated at or near the surface. Photomicrographs show dislocation pile up at sub-boundaries and bands of secondary slip on a $[111]$ surface.

A further study by Young (16) compared the different dislocation behavoir in annealed and irradiated copper crystals. He observed that in annealed crystals dislocation motion and multiplication occurred prior to macroscopic yielding. Relaxation effects were much greater for stresses less than the yield stress. For neutron irradiated crystals there was no motion or multiplication of dislocations prior to yielding.

More recently etchants have been developed which produce dislocation etch pits without an aging treatment. Liss (17) developed etch pits in iron in what appears to be glide bands. Pelosini and Allessandrini (18), also working on iron, demonstrated the increasing density of pits with work hardening, without intermediate aging treatment, on grains of all orientations.

A large body of literature now exists on the dislocation etching of metals. Well authenticated cases include the etching of busmuth (19), tungsten (20), nickel (21), molybdenum (22), zinc (23), cadmium (24) and niobium (25). A review of etching methods and etchants used is given by Bunshah (26).

Morphology of pits

Thus far the etch pit has been considered only as a marker which reveals dislocation sites and enables dislocation movements and interactions tp be plotted. But what factors affect the shape of the pit itself?

If the pit facets represent an equilibrium shape it would be necessary for a minimum to exist in the Gibbs-Wulff polar plot of surface free energy as a function of crystal surface orientation. If the facet

were planor this minimum would have to be a cusp. However, pit surfaces
are rarely planor and therefore do not correspond to cusped minima in the
Gibbs-Wulff plot.

It is probable that the kinetics of pitting control pit geometry
and that a thermodynamically stable shape is not attained. The model of
Gilman et al (27) and Cabrera (28) takes into account the nucleation of
mono-molecular steps at the intersection of the line defect with the
surface and the subsequent motion of steps away from this source.

In the two dimensional case shown in fig. 1 successive nucleation
of steps at the defect gives rise to a dissolution rate Vd at the defect.
Following nucleation, steps move out by removal of atoms successively
from certain preferred sites at the step edges, giving rise to an
independent velocity of pit widening Vs.

By an analysis of moving steps in terms of surface concentration
gradients, Hirth and Pound (54) predicted that a series of steps will
achieve a uniform steady velocity. Thus the slope of the pit will depend
upon the two independent parameters Vd and Vs. In practice pits of two
types are seen, conical and pyramidal, the latter reflecting the symmetry
of the crystal plane in which it lies. However, both types are nearly
always shallow with faces at angles not greater than 10° oriented from
the crystal surface. This fact explains why pits are often only found
on or within a few degrees of certain close-packed planes. The general
surface dissolution away from these surfaces is greater than the velocity Vd an
pits do not form. Truncation of pyramid shapes can be seen on planes close
to close-packed faces, e.g. on molybdenum single crystals (22).

It would appear then that close-packed, low index surfaces are normally the slowest etching and hence the most likely to be pitted. Whether or not a well defined pit will form appears to be determined by the rate of lateral spreading of the steps (the dissolving surface planes). Gilman et al (27) thought that this was controlled by the adsorption of impurity atoms or ions along the edges of the receding steps. Frank (29) and Cabrera and Vermilyea (30) then applied the theory of kinematic waves and showed that the role of adsorbed impurity was to promote bunching of the outward spreading steps so that sharp edge depressions were formed thus rendering the pit boundary clearly visible in the microscope.

This is substantiated by the work of Ives (51) who studied the effect of impurity concentration in the etchant on the morphology of pits formed on the $\{100\}$ cleavage surfaces of lithium fluoride. He showed that under conditions of diffusion control of dissolution pits took a conical shape but under conditions of surface kinetics control (detachment of atoms from the steps) pits had a square profile.

Some examples exist in the literature where pits are composed entirely of low index planes and yet undoubtedly originate at dislocation sites. Pits formed on $\{100\}$ and $\{112\}$ surfaces of tungsten single crystals (31) are shown to be bounded by crystallographically equivalent $\{110\}$ and $\{100\}$ faces, though somewhat rough in appearance.

Pits which appear to be composed entirely of low index facets have been produced on all orientations of polycrystalline lead by Gifkins and Corbett (32). Kauffman and Bardolle (33) definitely identify pits on pure iron single crystals as being composed of $\{110\}$ facets, their actual appearance being dependent on the orientation etched. They conclude that the pits are bounded by $\{110\}$ planes because these have the greatest atomic

density and hence the lowest surface free energy. They do not draw any conclusions as to the origin of the pits.

Recently Taoka et al (41) have developed etchants for several iron alloys, copper and zinc which produce pits bounded by low index planes and whose profiles, therefore, reflect the crystallography and orientation of the surface in which they lie. Using a goniomicroscope, the angles between the pit faces and the surface can be measured. If the poles of each face are set out on a polar stereographic net the orientation of the crystal surface is easily determined. Under good conditions the method is as accurate as the more conventional back reflection Laue X-ray method for orientation determination and is much simpler in operation.

Such pit shapes can be rationalised by considering them to be bounded by the slowest etching orientations, normally low index planes.

The kinematic theory of crystal growth and dissolution as developed by Frank(29) provides an opportunity to theoretically build up successive dissolution profiles, from independently determined dissolution data; and these can be compared with experimentally observed pit shapes to test the conditions responsible for pit morphologies.

Frank(29) used the model of fig. 1 to describe formally a crystal growth or dissolution process. The theory is two dimensional referring to a long prism or cylinder of crystal and the speed with which steps move depends, among other things, on the proximity of other steps. The speed is considered to be a function of step density alone and the methods used are those applied by Lighthill and Whitham(48) to problems of read traffic and river floods, in which also the flow (cars, or gallons, per minute) may often be assumed to depend only on the linear density (cars, or gallons, per mile).

Surface slope $=$ hk $=$ dy/dx

where k $=$ step density i.e. the number of steps per unit length in the neighbourhood of a particular point

Dissolution rate normal to the reference surface $=$ hq $=$ $-$dy/dt where q is the step flux i.e. the number of steps passing a particular point in unit time.

From the basic postulate

$$q = q(k)$$

we have two important velocities

$$v(k) = q/k; \quad c(k) = dq/dk$$

The first is the speed at an individual step; the second is called by Lighthill and Whitham the "kinematic wave velocity".

From the continuity equation (conservation of steps),

$$\frac{\partial q}{\partial x} + \frac{\partial k}{\partial t} = 0$$

we have

$$\frac{\partial q}{\partial k} \frac{\partial k}{\partial x} + \frac{\partial k}{\partial t} = 0$$

i.e.

$$c(k) \frac{\partial k}{\partial x} + \frac{\partial k}{\partial t} = 0$$

Thus in the (x, t) plane along a line of slope

$$\frac{dx}{dt} = c(k) = \frac{dq}{dk}$$

k is constant and therefore q is constant also.

Geometrically the sequence of crystal profiles $y = y(x)$ at a sequence of times t defines a surface $y = y(x, t)$. The characteristics correspond to lines on this surface, which we have just shown to have straight line projections on the (x, t) plane.

Consider now the projection on the (x, y) plane.

For this $$\frac{dy}{dx} = \frac{dy}{dx} + \frac{dy}{dt} \frac{dt}{dx}$$

$$= h (k - q/c) \text{ which is constant.}$$

The characteristics therefore project as straight lines on the (x, y) plane also. During dissolution, then, points of a given orientation have straight line trajectories (Theorem I).

A simple geometric construction from the graph of q v k gives the direction of the trajectory of a point of given orientation.

If the dissolution or growth velocity is measured normal to the actual surface of the crystal (rather than normal to a particular crystallographic plane) and the polar diagram of the reciprocal of this velocity formed, the trajectory of a point of given orientation on the crystal surface may be shown to be parallel to a normal to the polar diagram at the point of corresponding orientation. (Fig. 2) (Theorem II).

If the whole argument were conducted vectorially, it would be seen that it is also true in three dimensions though Frank provided proof only in the two dimensional case. The actual construction of the polar reluctance diagrams and the prediction of dissolution profiles from them is described under "Experimental Work".

The topographical theory of orientation dependent dissolution of crystals developed by Frank found its first experimental verification in the work of Frank and Ives (34) who used the experimental results of Batterman (35) on the dissolution of single crystal germanium.

Batterman measured etch rates in "Superoxol" etchant as a function of orientation along the $[1\bar{1}0]$ zone. Ives and Frank constructed a polar diagram of reciprocal etch rate and from this deduced the expected dissolution profile of a $\{100\}$ circular section of germanium. The derived profile was found to agree quantitatively with that obtained experimentally by etching out a hemispherical hollow on a $\{100\}$ surface.

To further test the applicability of Frank's theorems, Ives (36) etched away a square prism of lithium fluoride and, finding that dissolution trajectories were in fact straight lines, he constructed a reluctance diagram of reciprocal etch rate for the $\{100\}$ section. The diagram showed considerable anisotropy of etching. A profile for the dissolution of a cylindrical groove in a $\{100\}$ face of lithium fluoride was derived from this data and found to agree, at least qualitatively, with the profile obtained experimentally.

Hulett and Young (37) made a rigorous application of the kinematic theory of dissolution to copper crystal etching studies in order to interpret the evolution of the topography of the pits. The dissolution shapes of pits on $\{111\}$ surfaces at successive times were recorded by interference photomicroscopy. The evolution of the shapes was seen to be in accord with the predictions of the theory.

In extending this type of work to metals, Shemenski et al (38) showed that the dissolution kinetics of iron filamentary single crystals in dilute acid environments obeyed the topographical theorems proposed by Frank. They observed successive dissolution profiles of the tips of these whiskers in situ by using time-lapse motion picture photomicroscopy. Polar reluctance diagrams constructed from these profiles agreed well with experimentally determined dissolution rates.

Deduced etch pit profiles for both $\{110\}$ and $\{100\}$ faces were found to be identical to those observed on equivalent faces of the whiskers. A three-dimensional reluctance surface for iron whiskers having $\langle 111 \rangle$ growth axes inferred from the profiles was consistent with known relative magnitudes of anisotropic dissolution rates. The reluctance plots constructed according to the kinematic theory were seen to be two-dimensional sections of this surface.

The iron whiskers used in the present work were prepared by reduction of ferrous chloride in hydrogen according to the method devised by Brenner (39). Such whiskers in general have irregular shape and size but some can be grown up to several hundred microns in diameter and up to one centimetre long, having perfect crystallography with mirror like $\{100\}$ and $\{110\}$ faces.

Three types of these perfect whiskers are found (fig. 41) having the growth directions $\langle 111 \rangle$, $\langle 110 \rangle$ or $\langle 100 \rangle$. Coleman (40) etched such whiskers in both picral and nital and found that as grown, undeformed $\{100\}$ faces did not pit until dislocations were introduced by bending. ($\{110\}$ faces were uniformly attacked in both deformed and undeformed states). Dislocation motion and eventual arrangement in sub-grain boundaries was observed during annealing of deformed whiskers.

<u>The aims of the present work</u>

It was decided in the present work to investigate the nature of those pits bounded by low index facets produced by etching in the solutions developed by Taoka et al (41). Such pits appear to form quite randomly over all orientations of a polycrystalline surface, with no preference for any one type of site, and the questions arise, what factors control the nucleation and subsequent morphology of these pits? The present thesis is

an attempt to answer both these questions in the specific case of the crystallographic etch pitting of pure iron.

In the previous cases of etch pitting of metals the investigators have set out to show, sometimes not very convincingly, that their particular etchant produces pits only at dislocation sites. No one appears to have considered the possibility that a surface film could have some influence on the nucleation and growth of pits. And yet one of the important differences between non-metallic and metallic crystal surfaces is the common occurrence of an air formed oxide film on the latter. Aluminum for example has a tenacious oxide skin because of its strong affinity for oxygen.

Numerous studies have been made of the oxide formed at different temperatures on iron surfaces. Sewell et al (42) investigated oxide films formed at room temperature on iron single crystals and polycrystals by means of electron diffraction and electrochemical methods. The structure of the oxide was found to vary from an Fe_3O_4 type material at the metal/ oxide interface to a $\delta-Fe_2O_3$ type material at the oxide/air interface. The detailed nature of the film varied with the crystallographic orientation of the iron substrate, the mode of formation and the time of air exposure. The oxide formed as a highly oriented, compact array of micro-crystals of lateral extension less than 30 Å. Mean film thickness was in the range of 10-25 Å.

It was decided, in the present work,

(a) to study the growth morphology of the pits developed
by Taoka et al (41) on iron as a function of etching time
and etchant concentration;

(b)   to deduce etch pit profiles from a reluctance diagram whose reciprocal etch rates were derived experimentally from successive dissolution shapes of iron single crystal whiskers;

(c)   to compare these deduced profiles with observed etch pit shapes to determine the applicability of Frank's topographical theorems and hence whether pit morphologies are controlled by orientation dependent dissolution kinetics or not, and

(d)   to show what effect, if any, the presence or absence of an air-formed oxide film has on etch pit nucleation and morphology.

It will be shown that pit morphology is controlled by orientation dependent dissolution (after Frank) and that etching of an oxide free surface produces a dramatic change in pit nucleation and subsequent shape.

CHAPTER II

ETCHING POLYCRYSTALLINE IRON

In the following experiments the pure iron used was Ferrovac E vacuum melted iron. No free carbide was detectable in the structure though small quantities of inclusions were present. These latter etched out as holes during chemical polishing but proved to be of no inconvenience in the final analysis. Grain size varied from about 0.04 mms. up to about 0.5 mm.

The three etchants described in Table I were devised by Taoka et al (41) to produce large pits having well defined crystallographic facets. Sample surfaces were prepared for etching by mechanical polishing through grinding papers and diamond impregnated polishing cloths down to a one micron finish. A chemical polishing solution (Table I) was used to dissolve away the deformed surface layer introduced by mechanical polishing. After total immersion for two minutes the sample was removed and doused immediately in running water, then dried in an air blast. Any delay in washing, or the use of laboratory solvents for washing, left a surface film on the sample which prevented uniform attack on subsequent etching.

Etching was accomplished by total immersion, it being found unnecessary to swab or stir. Each etchant was taken in turn to decide on an optimum time before proceeding to the next. Times up to one minute in solution A (Table I); up to one minute in B and up to thirty seconds in C produced a variety of pit sizes and distributions. The relative sizes of pit facets could also be controlled. After etching in A pit shape was obscured by a reddish-brown oxide film covering the whole surface.

15

Etching in B removed this film but simultaneously changed pit shape and so to accurately determine the influence of solution A alone on pit shape certain samples were etched in A and the oxide film reduced by annealing at 875°C. for one hour in hydrogen.

The pits were photographed in their various stages of growth using a Zeiss Ultraphot optical microscope, a Zeiss interference microscope and a Cambridge Scanning Electron microscope (by courtesy of Dominion Foundries and Steel Company Ltd.). These studies, together with numerous measurements of pit facet angles with the goniomicroscope confirmed that the pits were bounded by $\{110\}$ and $\{100\}$ planes.

A diagram of the Unitron Goniomicroscope is shown in fig. 3. A pit in the grain whose orientation is to be determined is centralised using the micrometer stage. The vertical arm is then tilted while viewing through the eye-piece. The field goes dark but when the angle is reached at which the incident beam becomes normal to one side of the pit, that facet will reflect light to the observer's eye. The point of maximum brightness is estimated and the arm locked in position. Using the same principle, the stage is now rotated to achieve maximum reflection and locked. At this point the incident beam is absolutely normal to the facet in question and by reading off the two angles, arm (inclination) and stage (revolution) the position of the pole of the facet can be plotted on a polar stereographic net. The angles of only one more facet are needed to uniquely determine the orientation of the grain. For example, in the present case the two poles would be either $\{100\}$ or $\{110\}$ facets, square or hexagonal in appearance, respectively, and measurements along the great circles of the Wulff stereographic net gave the orientation of the centre of the projection (and hence of the grain) with respect to

the $\{110\}$ or $\{100\}$ planes.

Etch pit distribution and morphology.

Etching of Ferrovac E (annealed state, chemically polished) in solution A produced pits of uniform size (12μ diameter) evenly distibuted over the surface with no apparent preference for any one type of site. Occasionally pits appeared at grain boundaries. Surface dissolution appeared to be negligible and the sample became coated with a reddish-brown porous oxide film. This film was denser and darker over each pit, effectively masking its shape (fig. 4). If the surface were scratched lightly with the finger after chemical polishing pits would tend to form along the scratch. Pits did not form preferentially near heavily deformed areas, e.g. in the vicinity of a hardness impression.

As table III shows the number of pits was proportional to the time of etching. In this study it was impossible to distinguish between pits formed at an early time and those formed at a later time during etching as all pits were of a similar size. It would appear then that initially pits are nucleated at the most preferred sites and these grow rapidly to a maximum size where they are self passivated by the heavy oxide film cover formed. Pits then grow at not so highly preferred sites, and so on.

At long etching times the pits became so numerous and the oxide cover so thick that it was impossible to distinguish between pit and matrix. A photograph taken via the scanning electron microscope clearly shows the plates of oxide obscuring the pit, (fig. 5). Increase of hydrogen peroxide in etchant A caused an increase in the number of micro-pits in a given time but resulted in a decrease in their size.

When a sample is etched in A five seconds and the surface oxide removed by annealing in hydrogen the pits appear as in fig. 6 and fig. 7 (scanning electron microscope). It can be seen that the pits are bounded by {100} planes, the appearance of the pit depending on the orientation of the grain in which it lies.

A magnified image of an individual pit (S.E.M. fig. 8) shows that the {100} faces, ideally square, are in fact rounded and incipient planes of many other orientations are present, notably the {100} and {111} planes.

Standard samples prepared and etched five seconds in A were used to observe the effects of etchant B. The first five to ten seconds in this solution reduced the brown oxide film created by A. At longer times hexagonal shaped {110} planes began to appear at the corners of the {100} planes already present. These grew larger at the expense of the {100} facets.

Simultaneously, grain boundaries etched deeply and general surface dissolution occurred giving an overall roughening of the surface and a marked grain contrast. No new pits were nucleated. Extremely shallow, geometrically shaped, etch patterns or "figures" appeared on some grains at long etching times but it was not possible to relate these to crystal orientation in any way.

A pit etched five seconds in A and thirty seconds in B is shown on fig. 9 (S.E.M.). The rounded {100} facet is still in evidence and at its edges can be seen two roughly hexagonal shaped {110} planes. These can be grown until the {100} planes all but disappear. The rough appearance of the bounding faces of the pit is largely due to incomplete reduction of the porous oxide film.

Standard samples prepared and etched five seconds in A, one minute in B were etched for times up to one minute in solution C. The reaction was violent and accompanied by vigorous gassing. It was found that the pits grew to a maximum size of around thirty microns and that (110) planes were etched more rapidly than (100) with the end result that the pits ultimately became bounded by (100) planes.

The surface became much smoother and brighter after treatment in C and the pits extremely well defined, (fig. 10, S.E.B.). This figure shows clearly the way in which the pit profile changes with grain orientation. Note that certain pits have nucleated at grain boundaries and now straddle the boundary. They are in two distinct halves, each half reflecting the orientation of the grain in which it lies.

A close up of the pit in the centre of fig. 10 is shown in fig. 11. Note the perfect geometry and sharp bounding edges of the facets. The relative areas of the (110) and (100) facets are similar to those of the polyhedron sketched in fig. 40(a). Later etching times in solution C produced pit shapes corresponding to the polyhedron in fig. 40(b) and ultimately the (110) facets disappeared completely as in fig. 40(c).

Such pits are large enough for measurements to be made in the optical goniometer. Several pits were selected and the angles between the faces determined to be within two or three degrees of the true geometrical values. Many "finished" pits having different ratios of facet sizes are shown in figs. 12, 13, 14, 15 and 16, taken by interference microscope under thallium green light. The interference fringes are thus contours with a vertical interval of 0.27μ. By counting the fringes on a pit facet, and

knowing the magnification of the photograph, the angles between facets were determined approximately from a simple geometrical construction. The results confirmed those obtained by goniomicroscope work.

Effect of deformation on pit morphology

The above observations were made again using

(i) a deformed sample of Ferrovac E, finished by chemical polishing;

(ii) an annealed sample of Ferrovac E, finished by mechanical polishing only.

The results for the two different sample histories are basically the same. Etching in solution A produced pits uniformly distributed at sites apparently identical to those pitted on an undeformed sample surface. However, reduction in hydrogen revealed that the pit facets were all diamond shaped $\{110\}$ planes, the profile of the pit again reflecting the orientation of the matrix grain.

Etching in solution B merely increased the size of the pits, no new facets appeared and surface dissolution and grain boundary attack were similar to those on an annealed sample. Similarly, in solution C the pits grew larger with no change in morphology. In case (ii), the annealed and mechanically polished sample, it was difficult to distinguish the pit outlines at all because of rapid surface attack. However, at short times in C the diamond shaped $\{110\}$ planes were discernable, (figs. 17 and 18).

CHAPTER III

WHISKER DISSOLUTION

A batch of iron single crystal whiskers, prepared by Laukonis [J.V.] of General Motors Research Laboratories using the Brenner method (39), was examined, and whiskers having perfect geometry and uniform cross-section selected. The orientations of the bounding faces of several whiskers were determined by the etch pit method outlined above and the results confirmed using the standard back-reflection Laue X-ray technique, fitted with a narrow beam unit. The pitted (100) and (110) faces are shown in figs. 19 and 20 respectively.

Etch pits produced on (100) faces of the whiskers were identical to those produced on (100) grains of Ferrovac E, (fig. 19) but the (110) type etch pits tended to be blurred in outline (fig. 20). The odd few, however, did have perfect geometry.

Four whiskers were chosen, two having a (111) growth axis and two having a (100) growth axis, to determine the orientation dependent dissolution rate of pure iron in etchant C.

Each whisker was mounted in the jig shown in fig. 21. With the whisker tip just touching the surface of the liquid the set screw was turned two revolutions clockwise to lower the whisker 1/16 inch into the etchant. At each interval of one minute the whisker was lowered successive 1/16 inch distances until the available length had been used up (always leaving 1/16 inch of the whisker unetched to give the starting profile).

Top and bottom faces of the glass vessel were ground perfectly flat and parallel to mate with the flat top holding plate and a level section of bench respectively. The whisker was mounted perpendicular to the holding plate and the latter rotated slowly during dissolution in a rigid body movement, having an orbit diameter of approximately two inches. This was considered necessary, particularly at later dissolution times, because otherwise a red coloured reaction product tended to rise from the dissolving tip areas and collect at the meniscus surrounding the upper part of the whisker.

After dissolution, each whisker had a "stepped" longitudinal profile with each step uniform in cross section over more than half its length. The whisker was set vertically in the centre of a 3/4 inch diameter copper tube whose outside was circumscribed with rings spaced 1/16 inch apart and corresponding to the centre point of each "step". Cold mounting plastic was poured into the tube to hold the whisker for polishing. Short copper wires soldered to the inside of the tube served to key the inner plastic mount in place when set.

The whole mount was carefully ground down to each ring in turn and the whisker profile at each step in question prepared to a one micron finish by mechanical polishing. Each profile was photographed at a suitable magnification. Some difficulty was at first experienced in producing accurate, reproducible profiles, say of a whisker unetched and of uniform cross section, mainly due to flowing of metal and plastic during polishing. This problem was overcome by doubling the normal dose of hardener in the plastic (thus producing a harder mount) and by polishing with a very light touch. The resulting profiles for the two zones are shown in figs.22,23,24,25

Fig. 26 shows the actual series of dissolution profiles as photographed for whisker 16.

The etch rate of a particular orientation is then found as follows, (fig. 24). Set a rule at the required orientation and slide a 90° set square along the rule and draw tangents to each of the profiles in turn. The line joining the points of contact of tangent and profiles is a dissolution trajectory for a surface of that orientation and should, by Frank's first theorem, be a straight line. The normal dissolution rate is then the distance between the parallel tangents.

The two sets of dissolution profiles for the whiskers having $\langle 111 \rangle$ growth zones (figs. 22, 25) show a reasonably constant rate of etching. Although care was taken to select whiskers having perfect geometry and uniform cross section, impurity in homogeneities could have caused a variation in etch rate along the length of the whisker.

The profile of whisker 16 (fig. 23) shows that the original cross section, though composed entirely of $\{110\}$ planes, has three long sides of approximately equal length and three short sides of approximately equal length. The ratio of side lengths, taking side one as unity, for each profile, are given in Table 4. It can be seen that the sides approach each other in length as dissolution proceeds.

Table 5 gives the distances of the centre of each face from the centre of the section as a function of dissolution time. It is seen that despite the initial large variation in this distance, after five minutes it is almost exactly the same for all six faces, i.e. the whisker has become a symmetrically rounded hexagon. Thus side three which was initially the smallest of the six faces, and hence the fastest growing, is also the

fastest etching face. This demonstrates that crystal dissolution occurs by the same mechanism, in reverse, as crystal growth.

For a given profile, the centre of a face was taken to be the point of least curvature on that face. The centre of the section was the point at which lines joining centres of opposite faces crossed. These were found to be excellänt approximations as the six lines constructed all crossed at a point and intersected each other at sixty degree angles. (Forty-five degree angles in the case of the $\langle 100 \rangle$ growth zone).

The two sets of profiles of whiskers 18 and 7 (figs. 24 and 25), having $\langle 100 \rangle$ growth zones, although well defined, do not indicate such constancy of etch rate. Successive shapes do indicate a well ordered progression, however, to a section which is approximately square, rather than octagonal.

The somewhat distorted shape of whisker 18 after ten minutes reflects the inequalities in the original lengths of the small $\{110\}$ planes. Whisker 7 indicates this still more clearly. (Note the absence of a (110) plane at one corner and the slight rounding off of this angle as dissolution proceeds.)

As the absolute etch rates (table 6) show, there is excellent agreement between whiskers of the same growth zone. Agreement between the etch rate of $\{110\}$ planes of whiskers in different growth zones is not so good (the only orientation common to both zones). After observing the variation in etch rate between the faces of whisker 18, all of $\{110\}$ orientation, this is not surprising.

In drawing up the table of etch rates (table 7) all those values for equivalent crystallographic orientations were averaged to give one value per family of planes. The reciprocal etch rates used to construct the reluctance diagrams were related to the slowest etching orientation, i.e. $\{100\}$ as being unity.

The two polar reluctance diagrams of reciprocal etch rate versus orientation are shown in figs. 27 and 23. Etch pit profiles were predicted for the $\langle 100 \rangle$ growth zone (fig. 27) according to Frank's second theorem which states that the normal to the reluctance curve is parallel to the normal to the actual crystal surface at the corresponding orientation, i.e. is a dissolution trajectory. Thus the predicted profiles are determined as follows: Assume a circular starting profile and place a rule so that it touches the reluctance curve at the point corresponding to the orientation in question, i.e. it is a tangent. Place a 90° set square against the rule and slide it along until it intersects the starting profile at the same orientation. Scribe a line along the square. This is now the dissolution trajectory for that orientation. When similar trajectories are drawn for the other five degree intervals it will be seen that certain of them intersect. As it is physically impossible for trajectories to cross, they are erased beyond points of intersection and a line drawn through these points then represents an "edge" in the evolving etch pit.

To determine the actual shape of the growing pit we draw a tangent to the starting profile and side step the rule parallel to the tangent, along the dissolution trajectory corresponding to the orientation in question, for a distance equivalent to the known etch rate.

The smooth curve joining the limits so marked on each trajectory is then
the pit profile obtained after a certain time by etching a cylindrical
"hole" in a $\{100\}$ oriented grain of pure iron in solution C. In determin-
ing a profile only those trajectories which have not intersected an edge
are used. Any convenient scales can be used for the reluctance diagram
and the superimposed profiles, since it is only the <u>direction</u> of a diss-
olution trajectory that is required.

Two profiles for a growing etch pit are shown in fig. 27 for a
grain having $\{100\}$ orientation. At long times the profile becomes square
regardless of the darting shape. This is in agreement with the observed
effects of solution C on pits in Ferrovac E. (The point is discussed
more fully in the conclusions).

CHAPTER IV

ETCHING AN OXIDE FREE SURFACE

Samples of Ferrovac E were sub-critically annealed in hydrogen to reduce the oxide film and then were etched in solution A, still under a hydrogen atmosphere. Several investigators (49) (42) (5) have studied the reduction of oxide films on the surface of pure iron, checking for the presence or absence of a film by X-ray and electron diffraction methods. They consider that several minutes at 750°C. in hydrogen is sufficient to reduce any film present. In the present experiments a standard reduction treatment of half an hour at 875° was adopted.

Small specimens, about a half-inch diameter and one-eighth-inch thick, were given the standard mechanical polishing and chemical polishing treatment before reduction. The apparatus is shown in fig. 29. The specimen was pushed into the furnace hot zone, attached to the end of a nichrome wire, through the hydrogen flame at the end of the tube. After reduction it was drawn back into the cold zone where its temperature eventually dropped to no more than ten degrees above ambient.

To etch the sample in its oxide free condition, two small polythene vessels fixed to a copper base plate were fed through the flame into the cold zone. The first vessel contained solution A and the second distilled water for washing. The sample was dipped in the etchant then washed and returned to the reduction zone to remove the reddish-brown oxide layer produced during etching. This normally took one hour at 875°C.

The pits produced by this technique were entirely different both in distribution and morphology to those obtained during "normal" etching. A whole series of samples having a variety of pre-treatments was etched by this method and examined. The effect of etching time on pit morphology and distribution was studied. Samples plastically deformed in a vice before reduction are shown in figs. 30, 31 and 32. A sample prepared by mechanical polishing alone is shown in fig. 33. Fig 34 reveals the increased pit density near a diamond indentor impression.

Table 2 records pit counts on surfaces having a variety of pre-treatments. One sample was mechanically deformed after reduction but prior to etching, while still in the cold zone. This was achieved by allowing a pointed lathe tool, clamped to a 1/4 inch diameter steel rod, to fall from a height of 3/4 inch onto the surface of the sample. The impressions made on the surface were of similar size to those produced by a microhardness indentation.

Basically, two types of pit were observed:-

(a)   shallow depressions of irregular shape with ill-defined edges (fig. 32) and

(b)   deep conical pits having a well-defined rounded form (fig.35).

In addition a lightly deformed sample (figs. 30, 31 and 32) revealed the shallow type of pit forming continuous or semi-continuous grooves along slip lines. As would be expected in a body-centred cubic polycrystalline metal the slip lines are "wavy" in nature and may pass through several grains to end abruptly at the boundary of a grain unfavourably oriented for slip, beginning again on the far side of such a grain.

Fig. 34 shows a sample heavily deformed by a Rockwell C diamond indentor under 20 kg. load. Increased pit densities were noted throughout the whole sample but particularly in the immediate vicinity of the indentation.

The effect of etching time is apparent by comparing figs. 35 and 36 which show the same area after etching for two seconds and four seconds respectively. Obviously the sample had to be removed from the apparatus for photomicroscopy (fig. 35) then re-reduced over again before etching a further two seconds to obtain fig. 36. The pits in the two photographs show a one-to-one correspondence.

It is evident from the foregoing that the pits nucleate and grow at singularities in the crystal structure. Pit counts on samples having various mechanical and thermal histories (table 2) show that pit densities are close to those which would be anticipated if pits were formed at dislocation sites.

Of course, all dislocations would necessarily be in the "aged" condition, and the samples in the annealed state to some degree, because of the reduction treatment required before etching. In the experiment in which a sample was reduced and deformed under hydrogen atmosphere immediately prior to etching, no increased density of pits was observed in the vicinity of the indentation. It is likely then that the dislocations need to be aged before etching will reveal their presence.

Fig. 37 shows an undeformed area at low magnification. Apart from the obvious grain boundaries the pits are clustered in an interesting manner. Two nearly complete loops can be seen, one in the centre of the field and another in the bottom right hand corner. The rest of the pits are clustered in groups.

A lightly deformed sample prepared by mechanical polishing alone produced some interesting etch features. Firstly, (fig. 33) the overall pit density was increased and they were all of the same type, not so shallow as the shallow pits of the annealed samples and more definite in outline, though still irregular in shape. The larger slip bands were crossed by fainter slip traces (fig. 38) and many interesting "rosette" type clusters were observed (fig. 39). A marked grain contrast was evident but this was due to a variation in general surface dissolution between grains rather than a variation in pit density. Surface attack was so rapid in fact that after two seconds etching practically all the scratches left after mechanical polishing had disappeared. An attempt was made to correlate the "colour" of a grain with its orientation, as determined by further etching the sample in air and making optical goniometer measurements. There appeared to be no direct correlation.

On all samples, etching for times greater than five seconds developed crystallographic facets on the deep conical pits, identical to those on pits produced by etching in air. In the case of the shallow pits the rapid overall surface dissolution seemed to overtake pit growth and they gradually faded out. Similarly, the shallow grooves along slip lines gradually faded out too, but at discreet intervals along the traces concial pits appeared which eventually developed facets.

After a long etching time, then, the appearance of the pits on an oxide free surface was similar to that of pits produced by etching in A in air, followed by the reduction treatment. The two conditions could be distinguished by the observations that on an oxide free surface:-

(a) number of pits was independent of time;

(b)   pits also appeared at grain boundaries, and

(c)   there was a wide variation in pit size and extent

of facet development.

The pits in fig. 36 can be seen to be developing a definite
crystallography.

Some investigators have shown dislocations to be "punched out"
from a microhardness impression. This was tried in the present work but
no extra pits were observed near the impression.

CHAPTER V

DISCUSSION AND CONCLUSIONS

Pit morphology under normal etching conditions.

It is apparent from the results that Frank's topographical theorems are valid for the orientation dependent dissolution of iron filamentary crystals. From the dissolution data obtained, growth profiles can be predicted which agree closely with observed shapes on polycrystalline pure iron. No pretence is made that the dissolution data is accurate in any absolute sense. Even if the experimental technique were improved, a variation in etch rate for planes of similar orientation would still be observed (see whisker 16, fig 23). Furthermore, if this variation did not exist, absolute etch rates obtained by dissolving iron single crystal whiskers would hardly be applicable to growth shapes on polycrystalline iron of a different purity.

It is maintained, then, that averaged _relative_ orientation dependent dissolution rates are the important quantities and pit shapes have been successfully predicted with this in mind. No attempt has been made to introduce a time scale to the derived pit profiles of fig. 26. Shape (1) represents an early profile where the individual trajectories still control the curvature of the pit boundary. Eventually these trajectories meet to form two edges and the pit has the shape (2).

32

Ultimately, since the two edge trajectories are converging, the pit becomes square and bounded by {100} planes. Normally, when etching in solution C, the starting profile is already similar to that of (2) (the exact size of the {100} faces depending on the time in solution B) but the same principles apply whatever the initial profile. The circular starting profile of fig. 26 was chosen for convenience of construction.

The similar prediction of pit shapes in a grain of {110} orientation from whiskers 14 and 16 is rather more difficult as the pit bounding faces do not intersect the surface at right angles. A three dimensional reluctance diagram is needed and this could be constructed for all stages of pit growth if etch rates of all the common low index planes in the cubic system were known. Etch rates for those planes whose normals lie in the ⟨100⟩ and ⟨111⟩ zones have been determined but whiskers having ⟨110⟩ growth directions could not be found, although such whiskers have been grown by Coleman (40). Thus the etch rate for a {111} orientation is missing from the present data.

However, the absence of {111} faces on the single crystals would indicate that this orientation is fast growing and hence fast etching. It would not, therefore, influence the ultimate growth shape of a pit.

The three dimensional reluctance surface would predict a shape as in fig. 40 b for a time corresponding to profile (2). It is seen to be bounded by {100} and {110} faces, as would be a spherical "bubble" inside an iron crystal after etching from the inside out. The pit profile expected on the surface of a grain of any orientation can be deduced by cutting the figure with a plane inclined at that orientation and tracing the intersection

of the bounding surfaces on the plane. In this way the observed shapes of pits in fig. 13 (S.E.M.) can be rationalised.

A similar figure cannot be drawn for a time corresponding to profile (1) of fig. 26 because there may be an unknown peak in the reluctance surface orresponding to the orientation $\{111\}$.

There is a close parallel here between dissolution behavior in etchant C and that in etchant A. Both produce shapes in which the slowest etching surface is $\{100\}$ and will therefore have similar reluctance diagrams. Growth of pits in A ceases when a certain critical diameter is reached because of some passivation effect and the ultimate shape bounded entirely by $\{100\}$ faces is not attained. Close observation of fig. 7 (S.E.M.) shows a rounding of the $\{100\}$ faces and the more detailed image of fig. 8 reveals well-defined $\{110\}$ faces and small facets close to a $\{111\}$ orientation. It is possible then that the maximum pit size obtained in solution A represents a stage of pit growth equivalent to that of profile (1) (fig. 26) in which individual trajectories have not yet intersected to give the edges between $\{110\}$ and $\{100\}$ planes which control pit shape thereafter.

The influence of the oxide film on pit nucleation

It is apparent, then that under normal etching procedures pits form at defects in the oxide film, not in the underlying base metal. The fact that etch pit densities vary with etching time rules out the possibility of a one-to-one correspondence with dislocations. The pits are most likely to be formed at flaws in the oxide film. A metal oxide film is invariably in a state of stress because the oxide crystal structure, although related in orientation to the base, is usually different in type and lattice parameter to its parent metal and will therefore be in a state of tension or compression There may also be a variation in lattice parameter in the film itself (42).

Certain of these flaws are highly favoured sites and are attacked rapidly until blocked off by reaction products. The potential required for further attack is then higher than that required to nucleate and grow pits at not so favoured sites, and so on. Pits occasionally grew at grain boundaries. The fact that the oxide film is related in orientation to the iron substrate (42) may create a film discontinuity where the base becomes discontinuous, i.e. at the grain boundary.

Observation of the effect of long etching times on the pits produced on an oxide-free surface shows that they, too, eventually assume a crystallographic shape. It would seem that all that is required is for a "hole" of some description to be nucleated; the kinetics of the system dictate that ultimately the pit must be bounded by certain crystallographic facets.

The observation that pits bounded by crystallographic facets can be formed at defect sites is not necessarily a contradition of the work done by McAusland and Ives (52). They made an extensive survey of etch pitting at defect sites and concluded that pit slopes were governed by the ratio of Vd to Vs (fig. 1). As they point out, this does not preclude the existence of low index facets on defect etch pits. A necessary condition for such facets is that Vd be sufficiently greater than Vs to produce a ratio Vd/Vs which is greater than the tangent of the angle between the low-index facet and the surface being etched.

The pits obtained by etching an oxide-free surface, then, are most probably nucleated at defect sites in the metal. Pit densities are independent of etching time and are close to the values of dislocation densities

expected for annealed iron. Densities do increase with plastic deformation but this effect tends to be masked because of the high temperature reduction. treatment needed prior to etching.

Deformation after reduction, but prior to etching, did not produce increased pit densities, indicating that an aging treatment is necessary to decorate the dislocations. Low and Guard (43) aged their crystals before etching as did Hibbard and Dunn (14). Suits and Low (13) demonstrated the effects of aging silicon iron crystals on the density of pits before and after deformation. They concluded that carbon segregation was a necessary pre-requisite for etching.

Slip lines produced by deformation were broad and "wavy" in nature (figs. 30 and 31). They would often cross a grain boundary with hardly a change in direction and then end abruptly at the next, only to continue in a grain ahead. The slip lines etched out in continuous shallow grooves, similar to the ones observed by Brandon and Nutting (44) and by Low and Guard (43). The "wavy" nature of the slip lines results from the ability of the screw components of dislocations to move off the glide plane easily and from the large number of slip systems. Certain arrays, presumably of edge character, remain confined to straight lines despite the complex stress patterns which exist in polycrystalline materials.

Brandon and Nutting (44), who studied deformation in polycrystalline iron, examined thin metal films in the electron microscope for evidence of carbide precipitation at the slip lines. Precipitates were not seen and they concluded that the differential etching effect was attributable to segregation. According to Zener (45) the distortion energy of the iron lattice will be substantially reduced if clustering of intersitial atoms occurs.

If the substitutional atoms segregate to dislocations differential etching may occur, but Brandon and Nutting consider that an etched groove is more likely to represent a region where impurity is more homogeneously distributed than elsewhere. If the dislocations remaining in the slip bands have broken away from their impurity atmospheres, and the Zener platelets are dispersed by slip, then the slip band would be expected to be attacked more readily than the matrix and etch out as a shallow groove.

Alternatively, if a dislocation network lying parallel to and just below a surface has an impurity atmosphere and the rate of dissolution is high in the impure region, an etch groove may form along the dislocation. The grooves observed by Low and Guard (43) were decorated with carbon. Alternatively, the local elastic strain associated with a dislocation lying parallel to and just below a surface could cause the observed differential etching effect.

It has been observed that etching an oxide-free surface produces two different types of pit. The relatively deep conical pits of fig. 35 were never found in slip bands and constituted the majority of pits in a well annealed, undeformed sample. They are most likely formed at well aged dislocations of edge character which intersect the grain surface at a high angle. As fig. 36 suggests these defects extend well below the surface.

The other type of pit, however, is shallow, irregular in shape and ill-defined (fig. 32). Some of the slip bands in fig. 32 are not continuous and are seen to be strings of individual pits of this type. The shallow pits are of the same nature then as the "grooved" slip lines. Cross slip of the screw component of a dislocation loop lying on or just below

the surface would result in the irregular shapes observed. Low and Guard (43) made accurate observations of dislocation loops lying beneath "U" shaped etch pits in the electron microscope and confirmed the tendency of a screw component to move out of its original glide plane.

Perhaps the most convincing evidence that the shallow pits and slip line grooves are caused by individual dislocations, dislocation loops or tangled networks parallel to and just below the surface, is the fact that after etching for a time of four seconds in solution A (as in fig. 36) they have all but disappeared. At longer times they vanish completely and only the deep pits are left, which by this time have started to develop crystallographic facets. (The general surface attack by solution A on an oxide free surface is very rapid. It is comparable to that of etchant C in air.)

Polygonisation in single crystals of iron as revealed by etch pitting has been demonstrated by many investigators (14), (13), (47). No well authenticated case exists for similar structures in polycrystalline iron. No evidence of polygonisation was found in the present work.

Although Keh (46) has shown that subgrains do grow in polycrystalline iron during recovery and recrystallisation, these were not revealed by etch pitting in the present work.

CONCLUSIONS IN BRIEF

1. Pit morphology in this system can be adequately predicted from the Frank topographical theory, i.e. pit morphology is controlled by the kinetics of orientation dependent dissolution.

2. Under normal etching conditions pits nucleate at flaws in an air-formed oxide film.

3. When this oxide film is removed pits nucleate at singularites in the metallic structure which appear to be sites of intersection of aged edge dislocations with the surface. Shallow irregularly shaped pits outline slip lines and are probably caused by either the segregated impurity atmosphere of, or the strain fields associated with, dislocation networks lying parallel to and just below the surface.

REFERENCES

1. Frank, F. C.   Phil. Mag. 42 809 (1951)

    Cottrell, A. H.   Dislocations and Plastic Flow in Crystals,
                              Clarendon Press, Oxford, 1953.

    Read, W. T.   Dislocations in Crystals, McGraw Hill,
                              New York, 1953.

    Friedel, J.   Les Dislocations, Gauthiers-Villars, Paris, 1957.

2. "Crystal Growth"   Discussions Faraday Soc. 5 (1949)

3. Verma, A. R.   Nature 167 939 (1951)

4. Amelinckx, S.   Nature 167 939 (1951)

5. Dawson, I. M. and   Nature 167 476 (1951)
    Vand, V.

6. Forty, A. J.   Phil. Mag. 42 670 (1951)

7. Horn, F. H.   Phil. Mag. 43 1210 (1952)

8. Vogel, Pfann, Corey   Phys. Rev. 90 489 (1953)
    and Thomas

9. Vogel, F. L.   Acta. Met. 3 95 (1955)

10. Dash, W. C.   Journal App. Phys. 27 1193 (1956)

11. Gilman, J. J. and   Journal App. Phys. 27 1018 (1956)
    Johnson, W. G.

12. Suits, J. C. and   Acta. Met. 5 235 (1957)
    Low, J. R.

13. Pickering, H.   Acta. Met. 13 437 (1965)

14. Hibbard, W. B. and   Acta. Met. 4 306 (1956)
    Dunn, C. G.

15. Livingston, J. D.   "Direct Observation of Imperfections in
                              Crystals", Wiley, P. 115.

16. Young, F. W. Jnr.   Journal App. Phys. <u>33</u> No.12, 3553 (1962)

17. Liss, R. B.   Acta. Met. <u>7</u> (1959) P.231.

18. Pelosini, D. L. and   Energia Nucleare <u>14</u> No.2 99 (1967)
     Alessandrini, G.

19. Lovell, L. C. and   Journal App. Phys. <u>30</u> 234 (Feb. 1959)
     Wernick, G. M.

20. Berlec, I.   Journal App. Phys. <u>33</u> 197 (Jan. 1962)

21. Guard, R. W.   Trans. Met. Soc. AIME <u>218</u> 573 (June 1960)

22. Dasm G. C. and   Met. Res. Bull. <u>2</u> 487 (1967)
     Pratt, P. L.

23   Mikuriya   Jap. J. App. Phys. <u>6</u> 141 (1967)

24. Kratochvil, P. and   Acta. Met. <u>14</u> 1757 (Dec. 1966)
     Homola, J.

25. Zedler   Journal App. Phys. <u>38</u> 2046 (April 1967)

26. Bunshah, R. F.   Techniques of Metals Research, Volume 2,
                                Chapter II. Interscience N.Y. 1968.

27. Gilman, Johnston and   Journal App. Phys. <u>29</u> 747 (1958)
     Sears

28. Cabrera, N.   "The Surface Chemistry of Metals and
                                Semi-conductors". Wiley, 1960.

29. Frank, F. C.   "Growth and Perfection of Crystals",
                                Wiley, 1958 P. 411.

30. Cabrera, N. and   "Growth and Perfection of Crystals",
     Vermilyea, D. A.   Wiley, 1958 P. 393.

31. Schadler, H. W.   "Direct Observation of Imperfections
                                in Crystals", Wiley, P. 593.

32. Grifkins, R. C. and   Laboratory Methods <u>74</u> No. 445 November 1966
     Corbett, J.A.   P. 239.

33. Kauffmann, J. P. and   C. R. Acad. Sc. Paris, t.266 439 (12 Feb. 1968)
     Bardolle, J.

34. Frank, F. C. and   Journal App. Phys. <u>31</u> 1996 (1960)
     Ives, M. B.

35. Batterman, B. W.   Journal App. Phys. $\underline{28}$ 1236 (1957)

36. Ives, M. B.   Journal App. Phys. $\underline{32}$ 1534 (Aug. 1961)

37. Hulett, L. D. Jnr.   Journal Phys. Chem. Solids $\underline{26}$ 1287 (1965)
     and Young, F. W. Jnr.

38. Shemenski, Beck and   Journal App. Phys. $\underline{36}$ 3909
     Fontana

39. Brenner, S.   Acta. Met. $\underline{4}$ 62 (1956)

40. Coleman, R. C.   Journal App. Phys. $\underline{29}$ 1487 (1958)

41. Taoka, T.   Jap. J. App. Phys. $\underline{4}$ 120 (1965)
     Furubayashi, E. and
     Takeuchi, S.

42. Sewel, Stockbridge   J. Electrochemical Soc. $\underline{108}$ 933 (1961)
     and Cohen

43. Low, J. R. and   Acta. Met. $\underline{7}$ 171 (1959)
     Guard, R. W.

44. Brandon, D. G. and   Acta. Met. $\underline{7}$ 101 (1959)
     Nutting, J.

45. Zener, C.   Phys. Rev. $\underline{74}$ 639 (1948)

46. Keh, A. S.   "Direct Observation of Imperfections
                             in Crystals", Wiley (1961) P.213.

47. Dunn, C. G.   Acta. Met. $\underline{3}$ 409 (1955)

48. Lighthill, M. J. and   Proc. Roy. Soc. $\underline{229}$ (A) 281, 237 (1955)
     Whitham, G. B.

49. Laukonis and Coleman,   J. App. Phys. $\underline{32}$ 242 (1961)

50. Sewel, Brewer, Cohen   J. Phys. Chem. $\underline{67}$ 2008 (1963)

51. Ives, M. B.   Industrial and Engg. Chemistry P.34 (June 1965)

52. McAusland, D.D. and   Surface Science $\underline{12}$ 189 (1968)
     Ives, M. B.

53. Bondi, A. A.   Chem. Rev. $\underline{52}$ 417 (1953)

54. Hirth, J. P. and   J. Chem. Phys. $\underline{26}$ 1216 (1957)
     Pound, G. M.

TABLE 1

Etchant A	HCL	1	Time	0 - 60 secs.
	H_2O_2	5		
	H_2O	100		

Etchant B	Saturated aqueous solution of		Time	0 - 60 secs.
	$Fe\ Cl_3 \cdot 6H_2O$	1		
	H_2O	5		

Etchant C	HCOOH	1	Time	0 - 60 secs.
	H_2O_2	1		
	H_2O	1		
	C_2H_5OH	1		

Largest size of pits compatible with even distribution and good definition of facets obtained by immersion two seconds in A, thirty seconds in B and five seconds in C.

Chemical polishing solution:		Time	2 minutes.
H_2O_2	8		
Phosphoric acid	10		
Ethanol	1		

TABLE 2

Condition	Pit Density
Annealed Ferrovac E	$0.25 \times 10^6 \text{ /cm}^2$
Mechanically polished surface	$0.6 \times 10^6 \text{ /cm}^2$
Deformed by Rockwell C indentor (average value)	$0.9 \times 10^6 \text{ /cm}^2$

TABLE 3

Effect of etching time in solution A

Time (secs.)	Number of Pits in field of view
2	18
4	45
8	89
16	147
32	254

Approximately three grains in field.

TABLE 4

Ratio of side lengths of whisker 16 taking side 1
as unity.

Side Number	1	2	3	4	5	6
Unetched	1	1.65	.85	1.65	1.00	1.45
1 min.	1	1.95	.85	1.95	1.05	1.70
2 min.	1	2.00	.80	2.00	1.05	1.85
3 min.	1	2.10	1.00	2.05	1.15	1.90
4 min.	1	1.55	.95	1.70	1.10	1.80
5 min.	1	1.30	.95	1.45	1.00	1.45

TABLE 5

Distances of centres of each face from centre of
section of whisker 16 (Magnification x 256) in cms.

Side Number	1	2	3	4	5	6
Unetched	4.85	4.15	5.20	4.15	4.85	4.25
1 min.	4.20	3.40	4.35	3.40	4.20	3.65
2 min.	3.65	2.90	3.65	3.00	3.60	3.10
3 min.	3.15	2.70	3.30	2.70	3.20	2.70
4 min.	2.50	2.20	2.45	2.20	2.50	2.25
5 min.	1.70	1.65	1.70	1.55	1.65	1.55

TABLE 6

Comparison of absolute etch rates for $\langle 100 \rangle$ and $\langle 111 \rangle$ growth zones of all four whisker profiles.

Whisker	{100}	{110}
16	—	23.0 ± 2.3 μ/min.
14	—	25.0 ± 2.5 μ/min.
7	11.0 ± 1.1 μ/min.	14.5 ± 1.5 μ/min.
18	12.0 ± 1.2 μ/min.	15.0 ± 1.5 μ/min.

TABLE 7

Etch reluctance versus orientation in degrees from {110} compared to {100} rate as unity, for whisker 18.

Degrees from {100}	Etch reluctance
0	1.00
5	.88
10	.83
15	.79
20	.77
25	.75
30	.75
35	.77
40	.78
45	.80

TABLE 8

Reciprocal etch rate versus orientation
in degrees from $\{110\}$ compared to $\{100\}$
rate as unity, for whisker 14.

0	.80
5	.74
10	.70
15	.67
20	.65
25	.64
30	.63
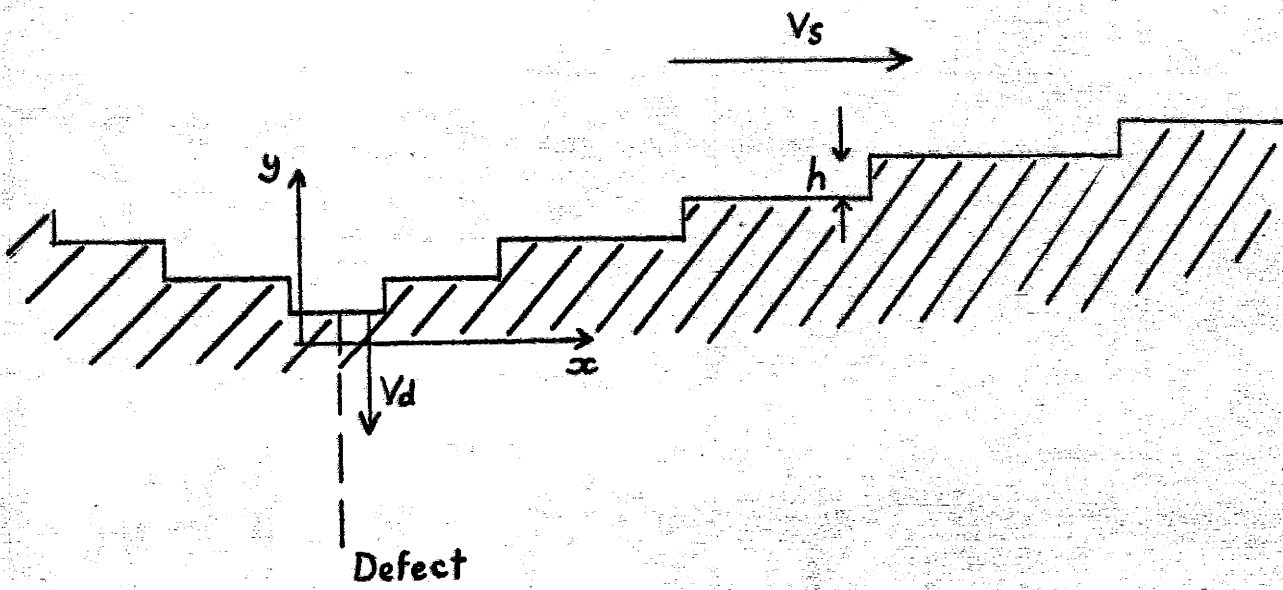
Fig. 1:   Two dimensional pit growth at a line defect.
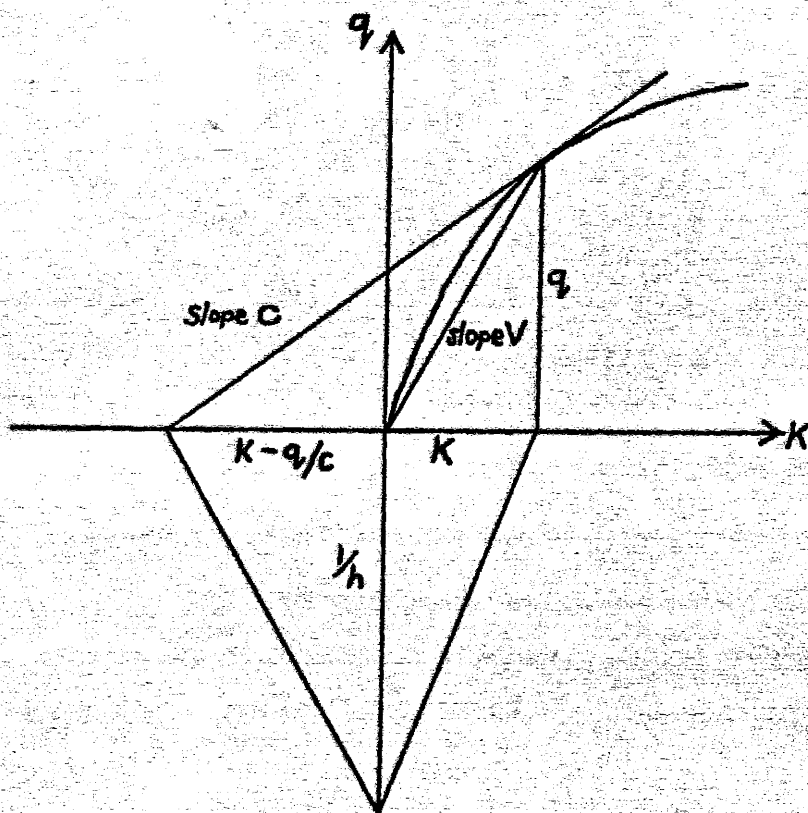
Fig. 2(a) The relationships of the parameters in the Frank theory of crystal growth and dissolution.
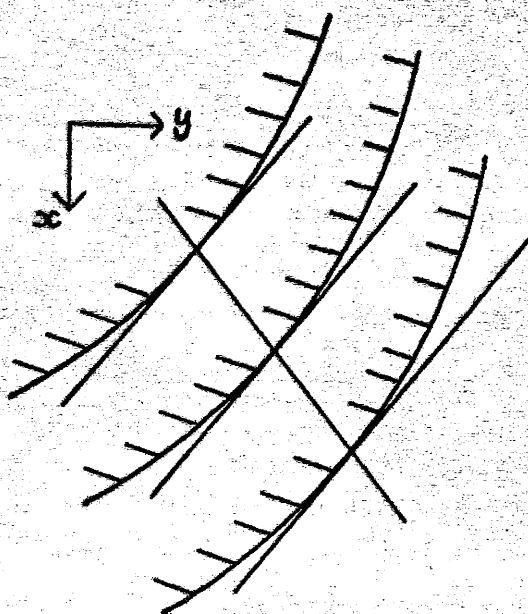
Fig. 2(b) Showing a straight line trajectory joining positions of the same orientation on successive dissolution or growth surfaces of a crystal.
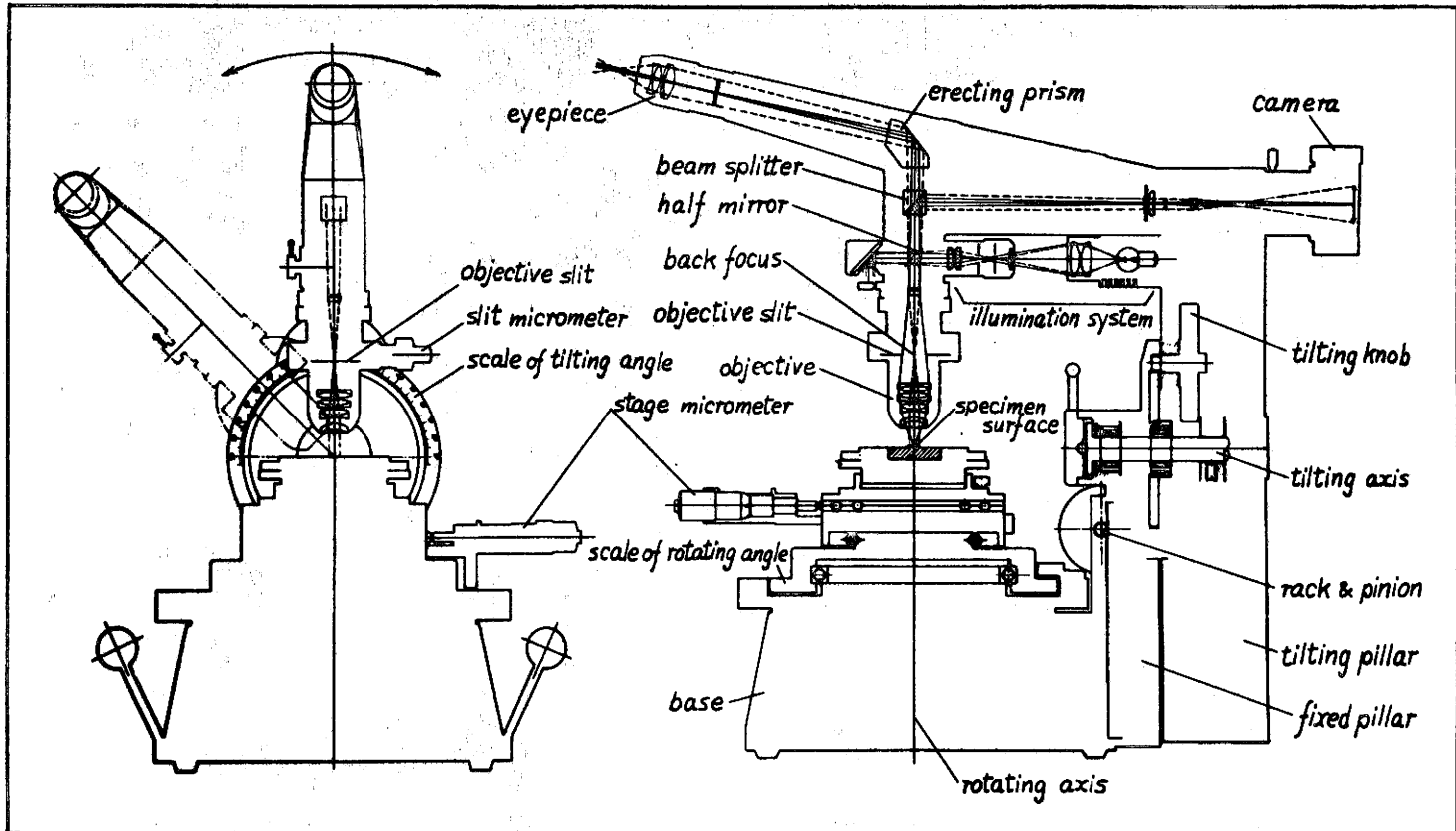
Fig. 3:   Goniomicroscope.
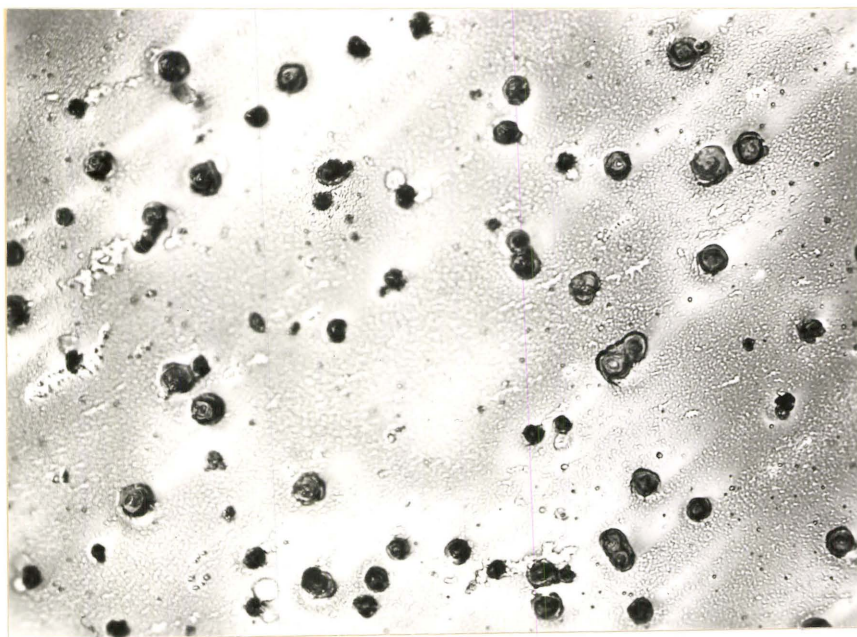
Fig. 4:   Pits after etching five seconds in A (showing oxide film) X 600.
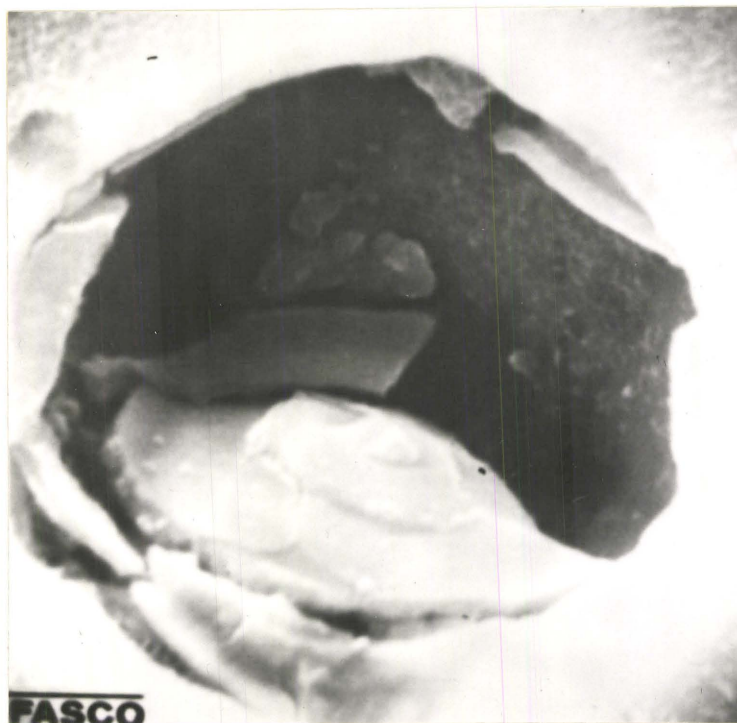
Fig. 5:   Pit covered with oxide as in fig. 2. Scanning Electron
            Microscope X 10,000.
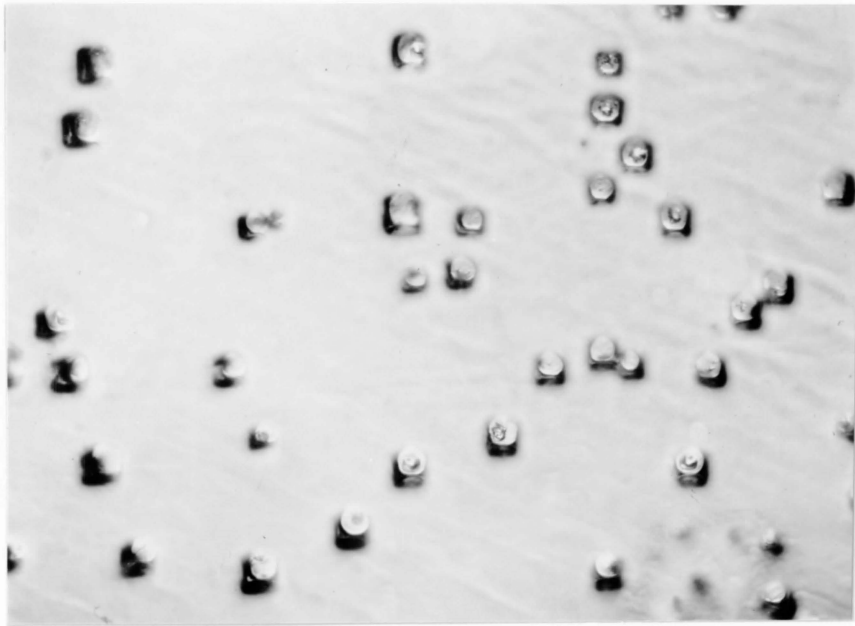
Fig. 6:   As fig. 2 with subsequent reduction in hydrogen at 875°C.
            for one hour X 400.
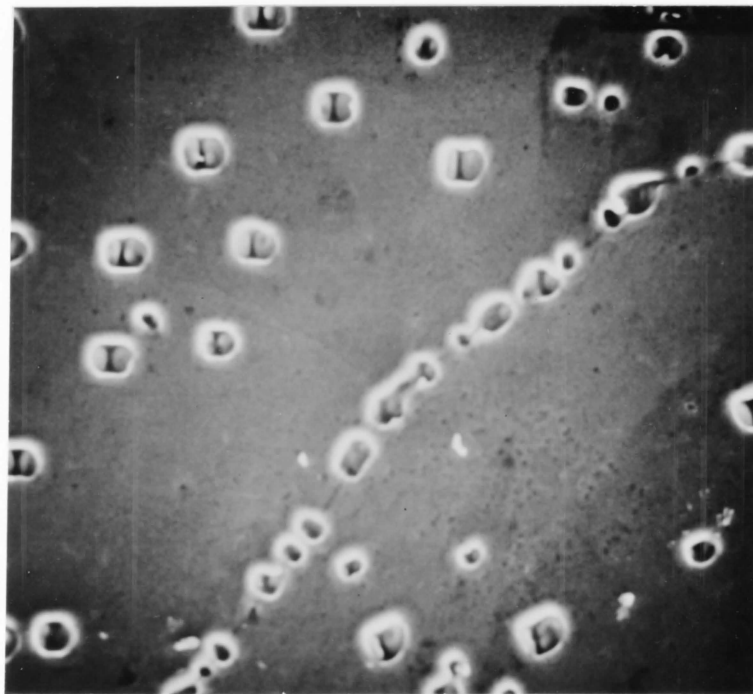
Fig. 7   As Fig. 6.   Scanning Electron Microscope X 500.
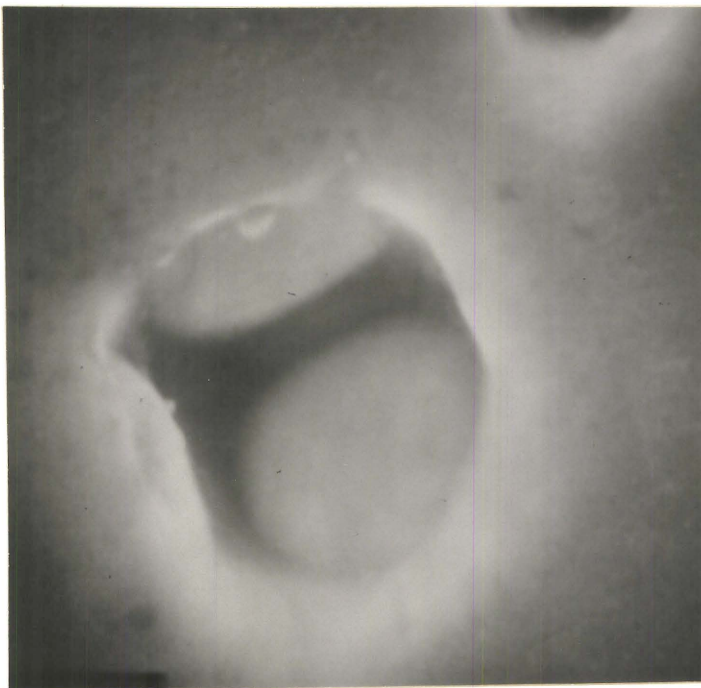
Fig. 8   As Fig. 6.   Scanning Electron Microscope X 5,000.
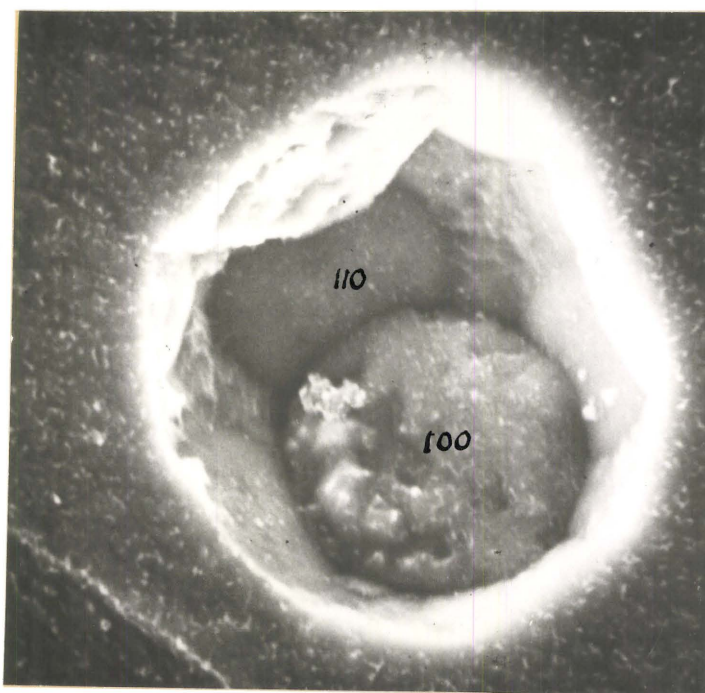
Fig. 9   Pit etched five seconds in Solution A, thirty seconds in Solution B.   Scanning Electron Microscope X 5,000.
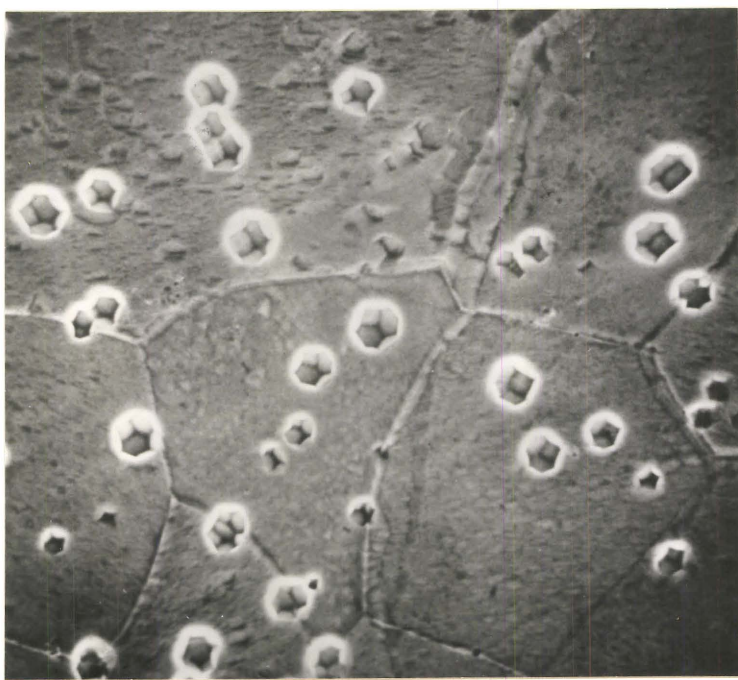
Fig. 10   Pits produced after etching in Solutions A, B and C.
           Scanning Electron Microscope X 500.
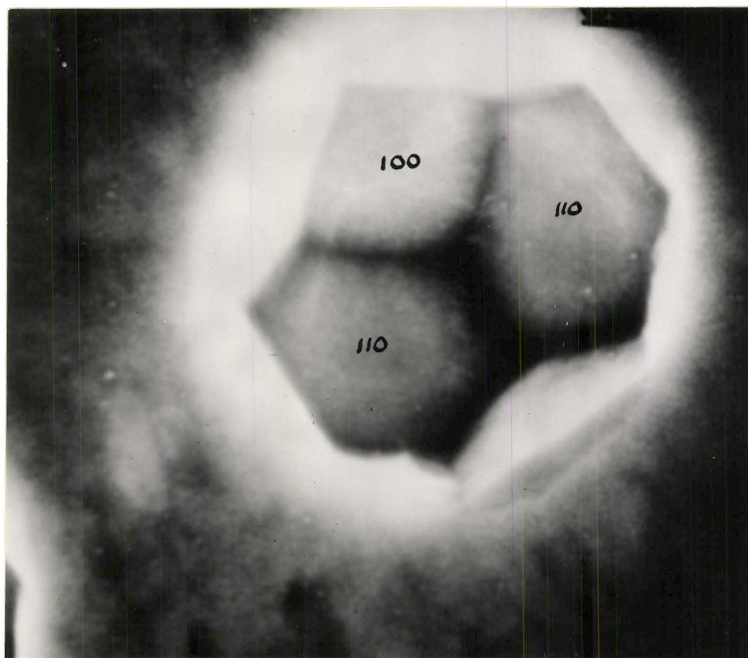
Fig. 11   Close up of pit in Fig. 10. Scanning Electron Microscope X 5,000.
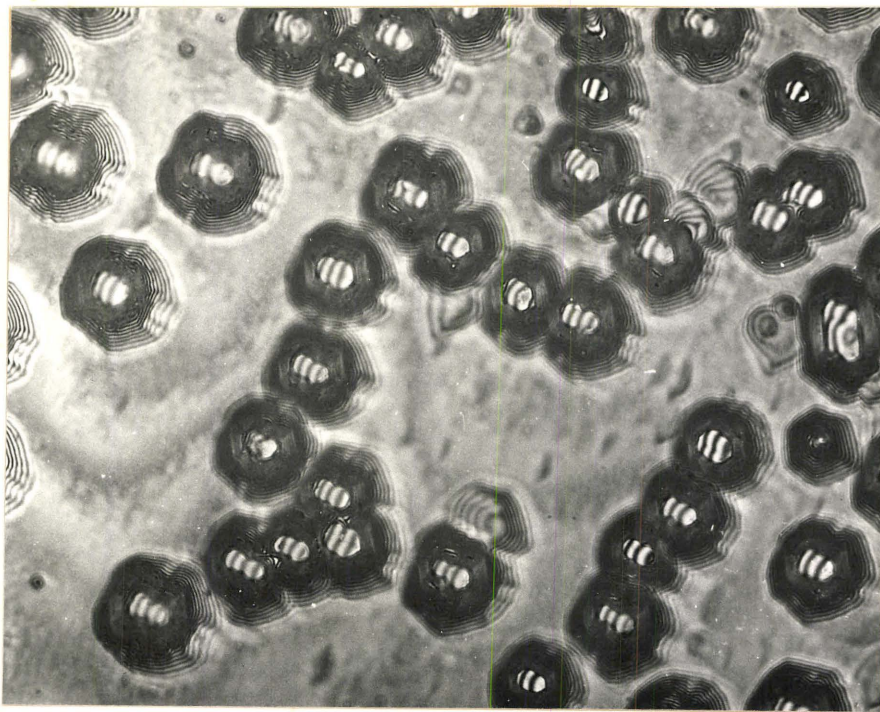
Fig. 12.   Pits etched in Solutions A, B and C and photographed via
an interference microscope X 400.
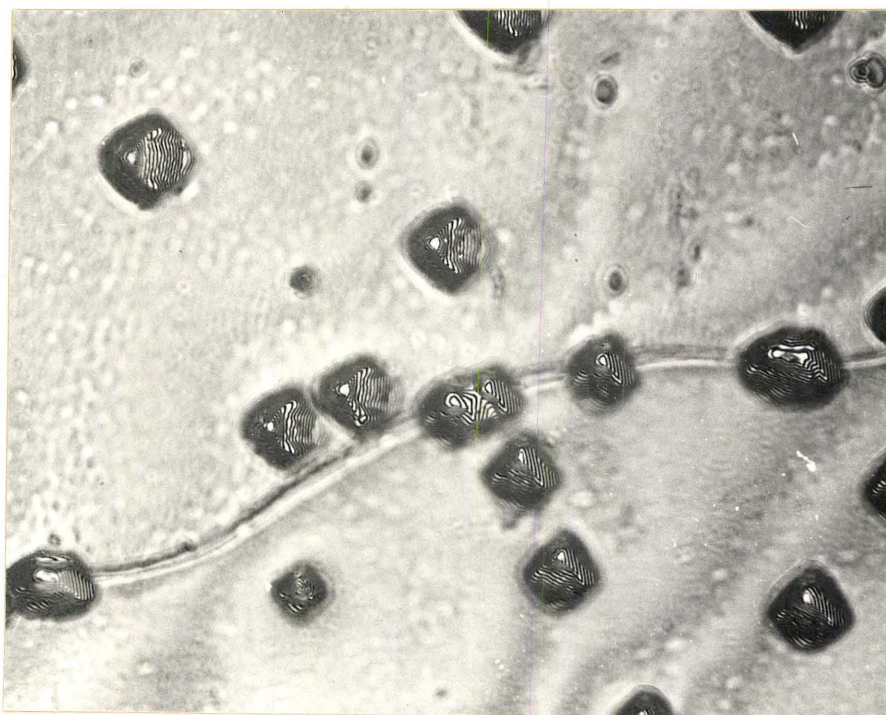
Fig. 13   As fig. 12.
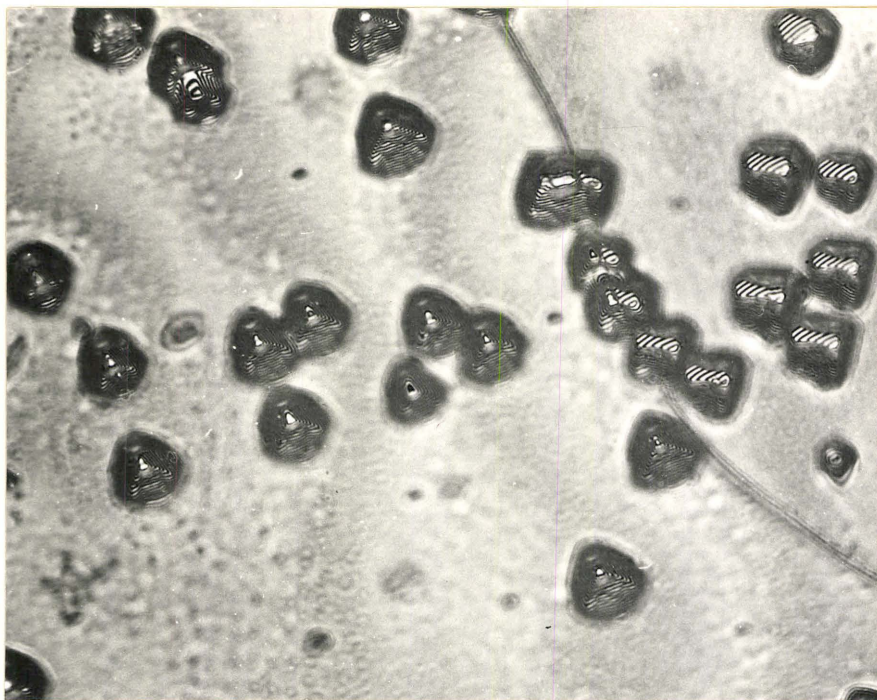
Fig. 14   As fig. 12
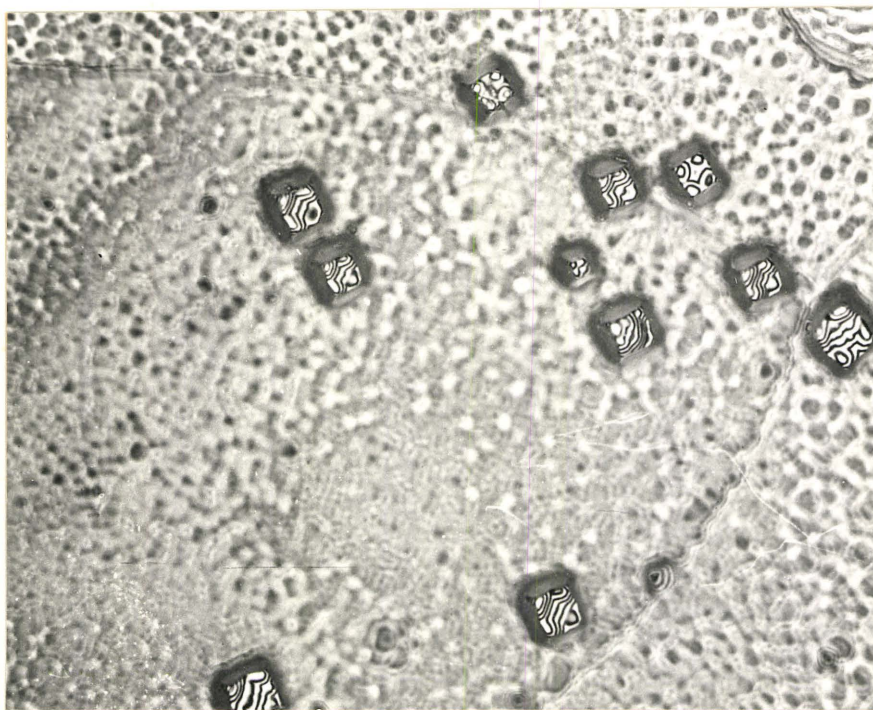
Fig. 15   As fig. 12.
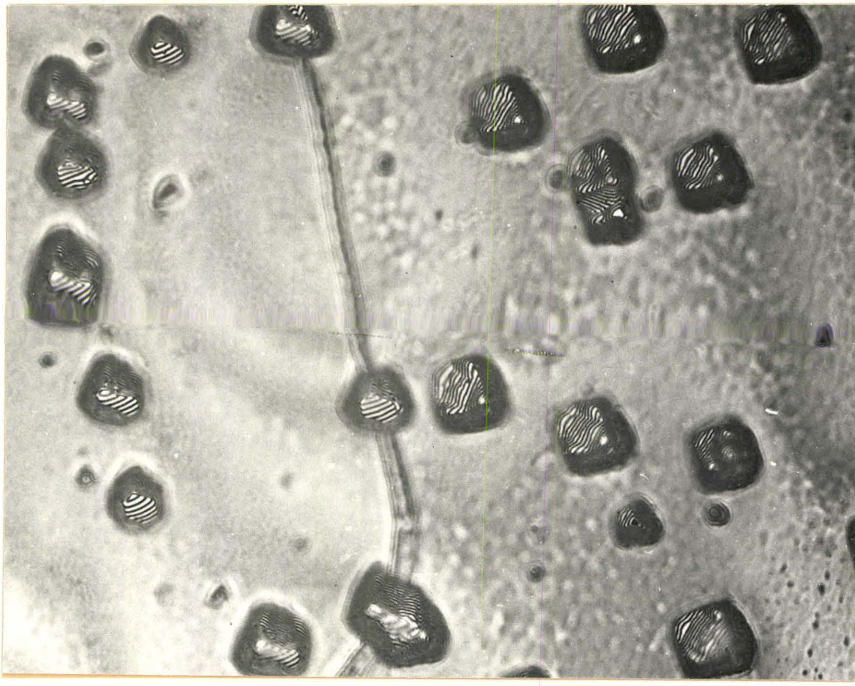
Fig. 16   As fig. 12
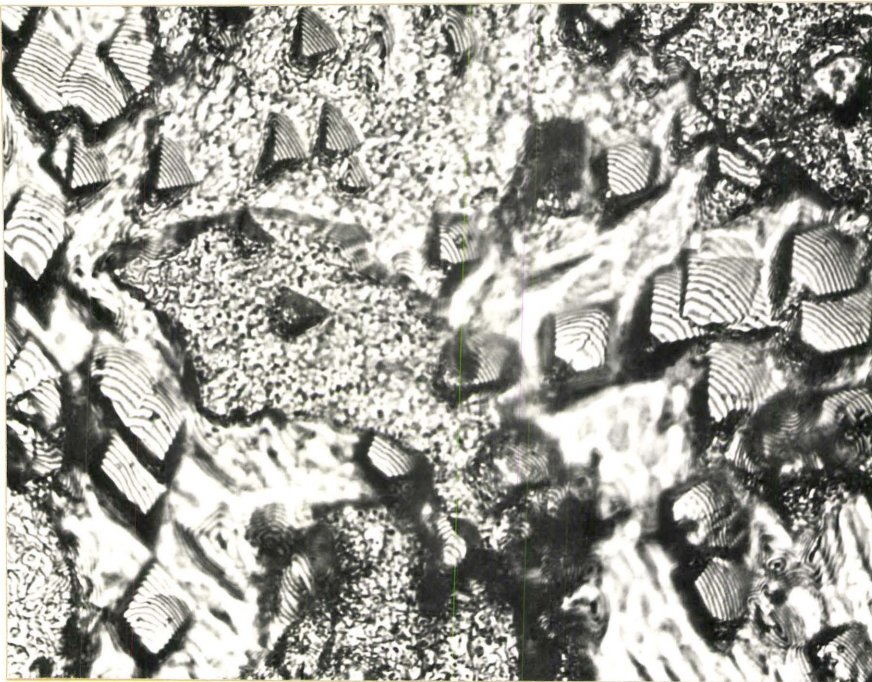
Fig. 17   Pits produced on mechanically polished sample by etching
in Solutions A, B and C   X 400

Fig. 18   As Fig. 17.
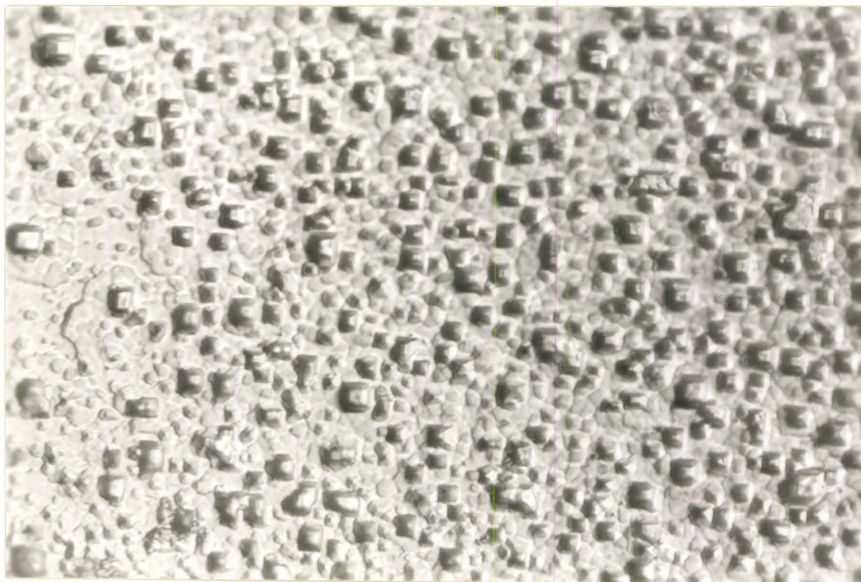
Fig. 19   Pits on 100 face of iron single crystal whisker X 1,200.
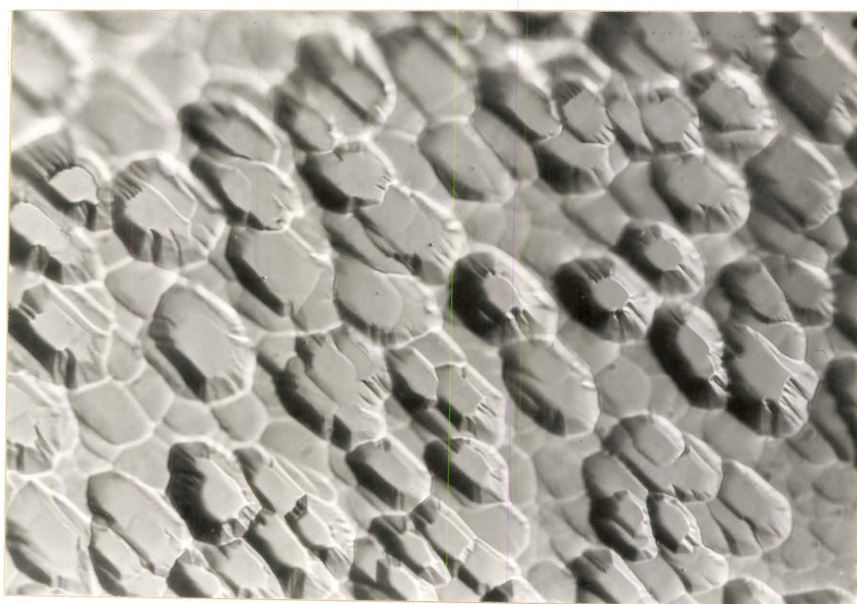
Fig. 20   Pits on 110 face of iron single crystal whisker X 1,200.
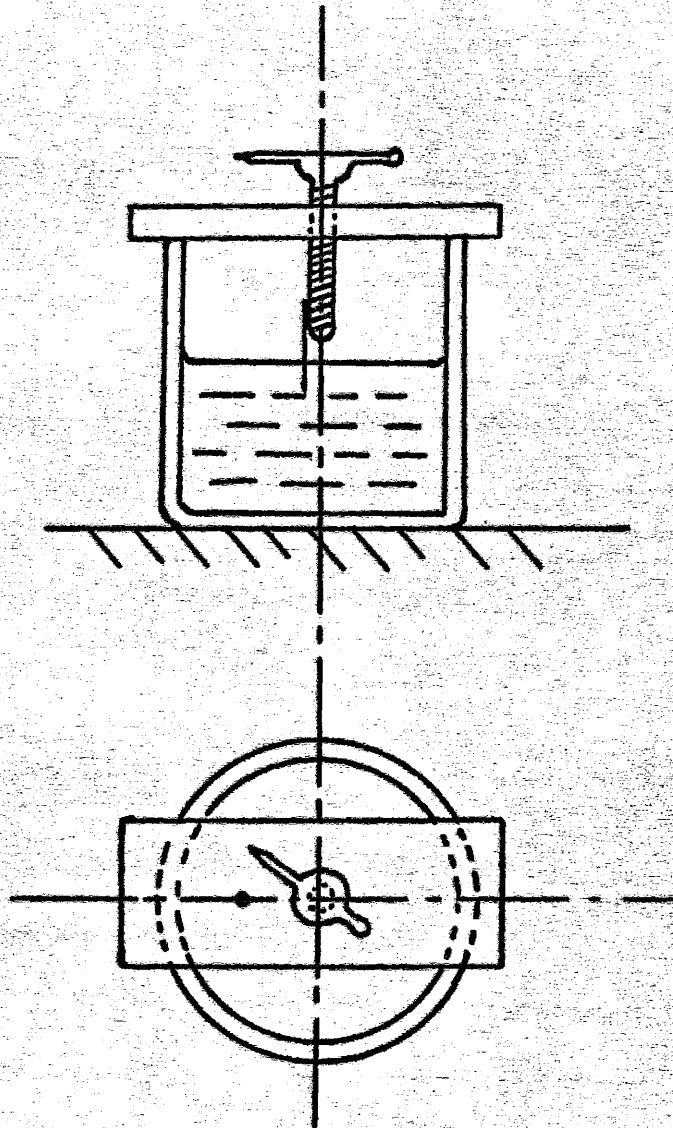
Fig. 21:   Apparatus used in whisker dissolution experiments.
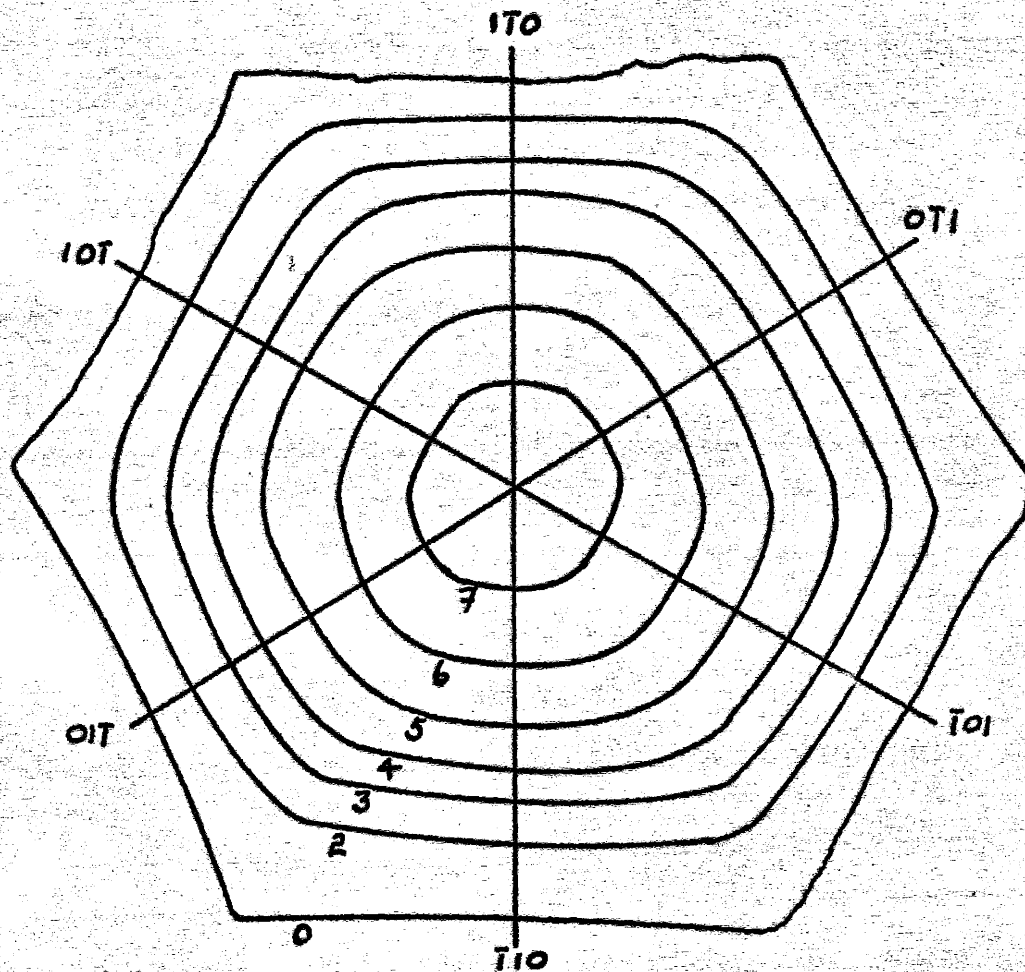
Fig. 22: Successive dissolution profiles of whisker 14 etched in solution C. The growth axis is the ⟨111⟩ direction. Profile numbers correspond to dissolution time in minutes. Magnification X 252.
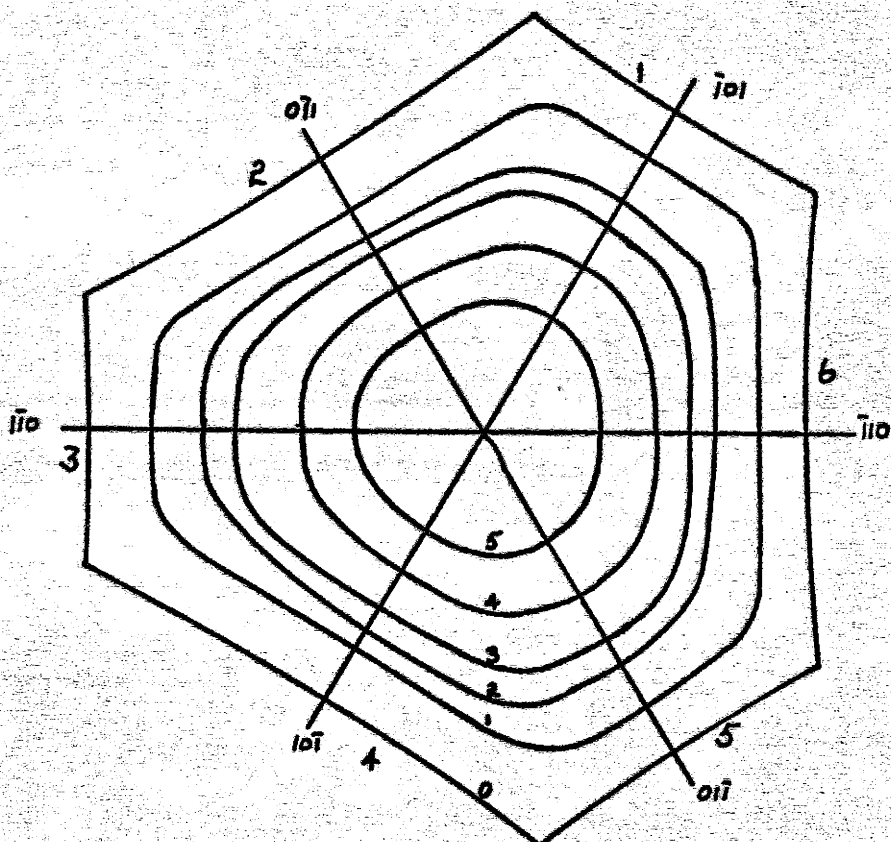
Fig. 23: Successive dissolution profiles of whisker 16 in solution C. Growth axis is ⟨111⟩ direction. Profile numbers correspond to dissolution time in minutes. Side numbers refer to Table 4. Magnification X 256.
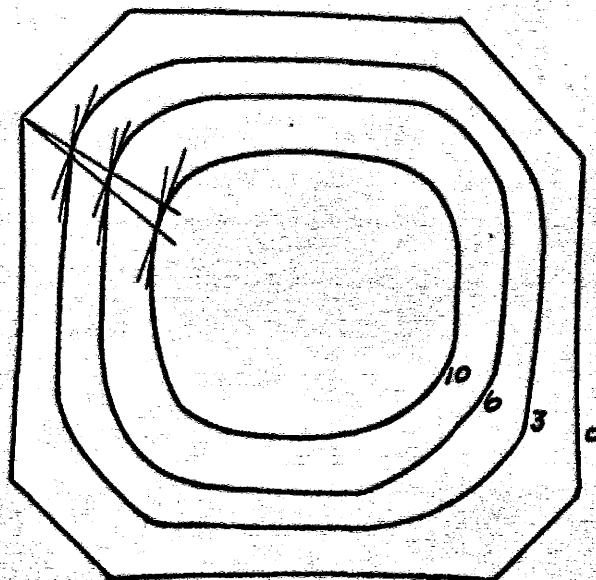
Fig. 24:   Successive dissolution profiles of whisker 18 in solution C.
Growth axis is ⟨100⟩ direction. Profile numbers correspond
to dissolution time in minutes. Two dissolution trajectories
are shown for two orientations lying 10° apart.
Magnification X 137.
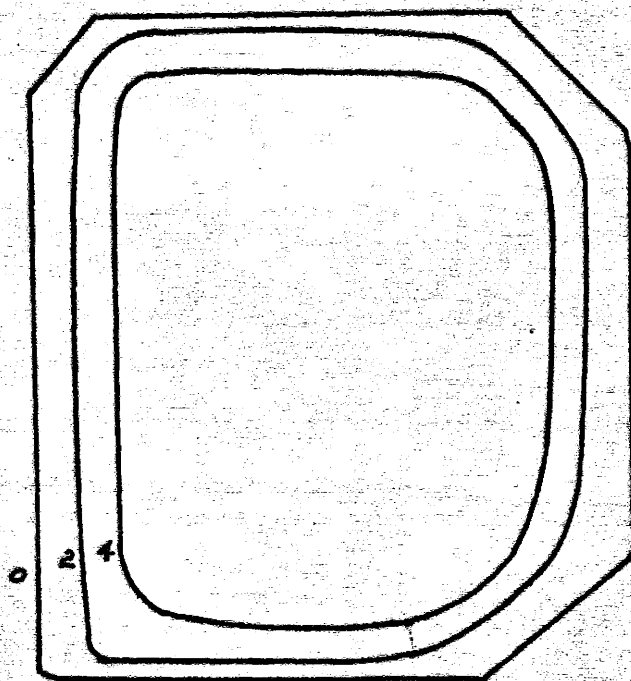
Fig. 25: Successive dissolution profiles of whisker 7 in solution C. Growth axis is ⟨100⟩ direction. Profile numbers correspond to dissolution time in minutes. Magnification X 200.
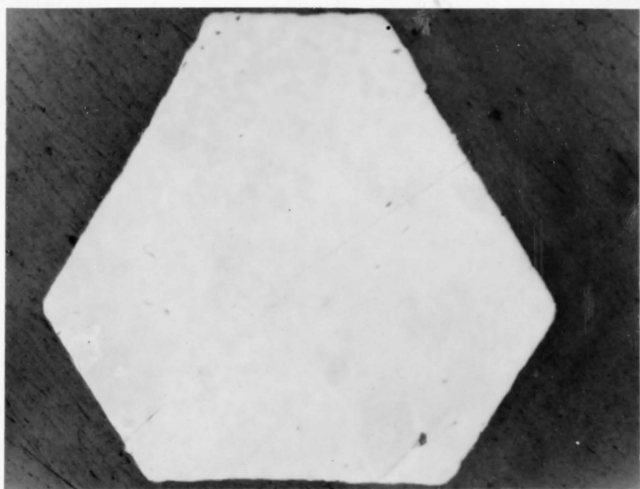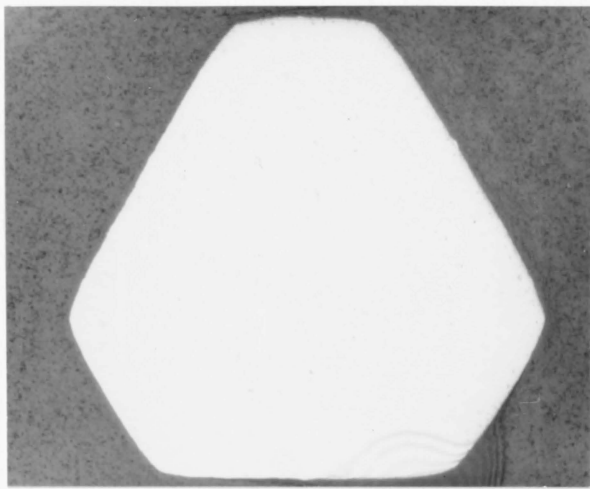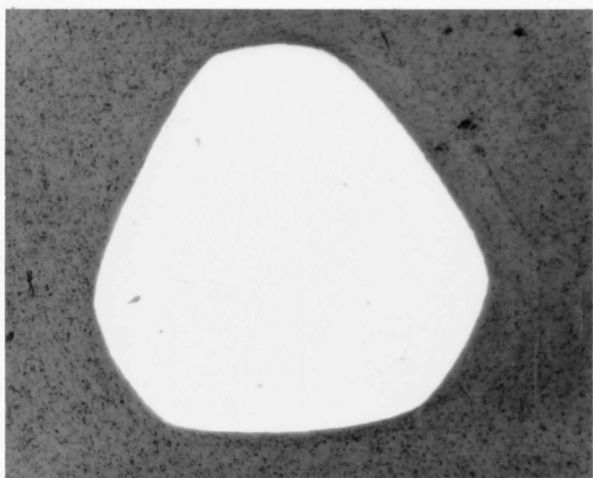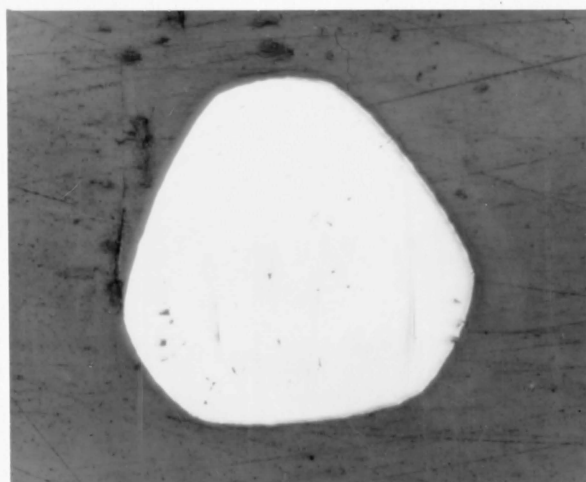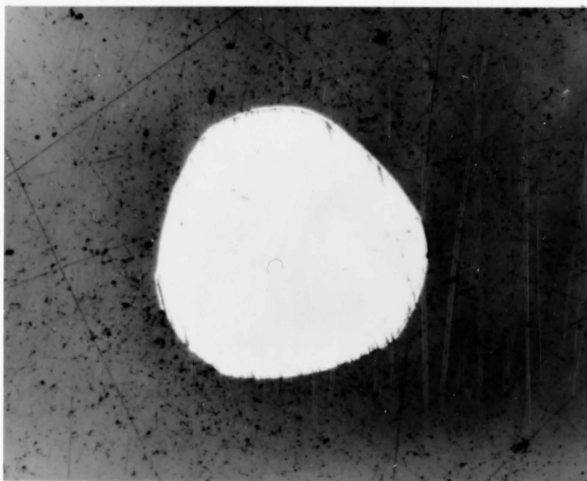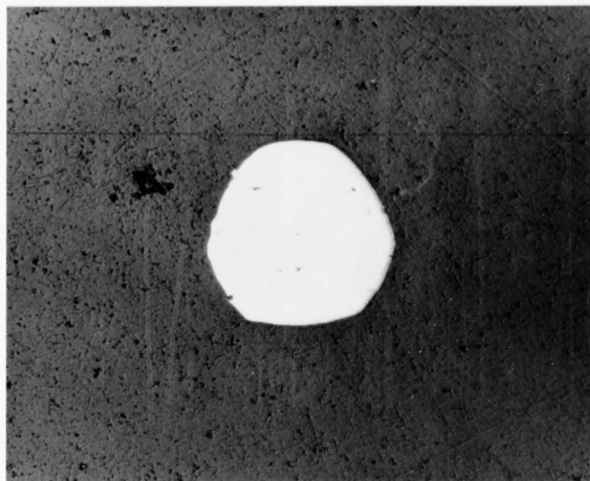
Fig. 26   Successive stages in the dissolution of whisker 16 (having
           111 growth direction). Numbers represent time in minutes.
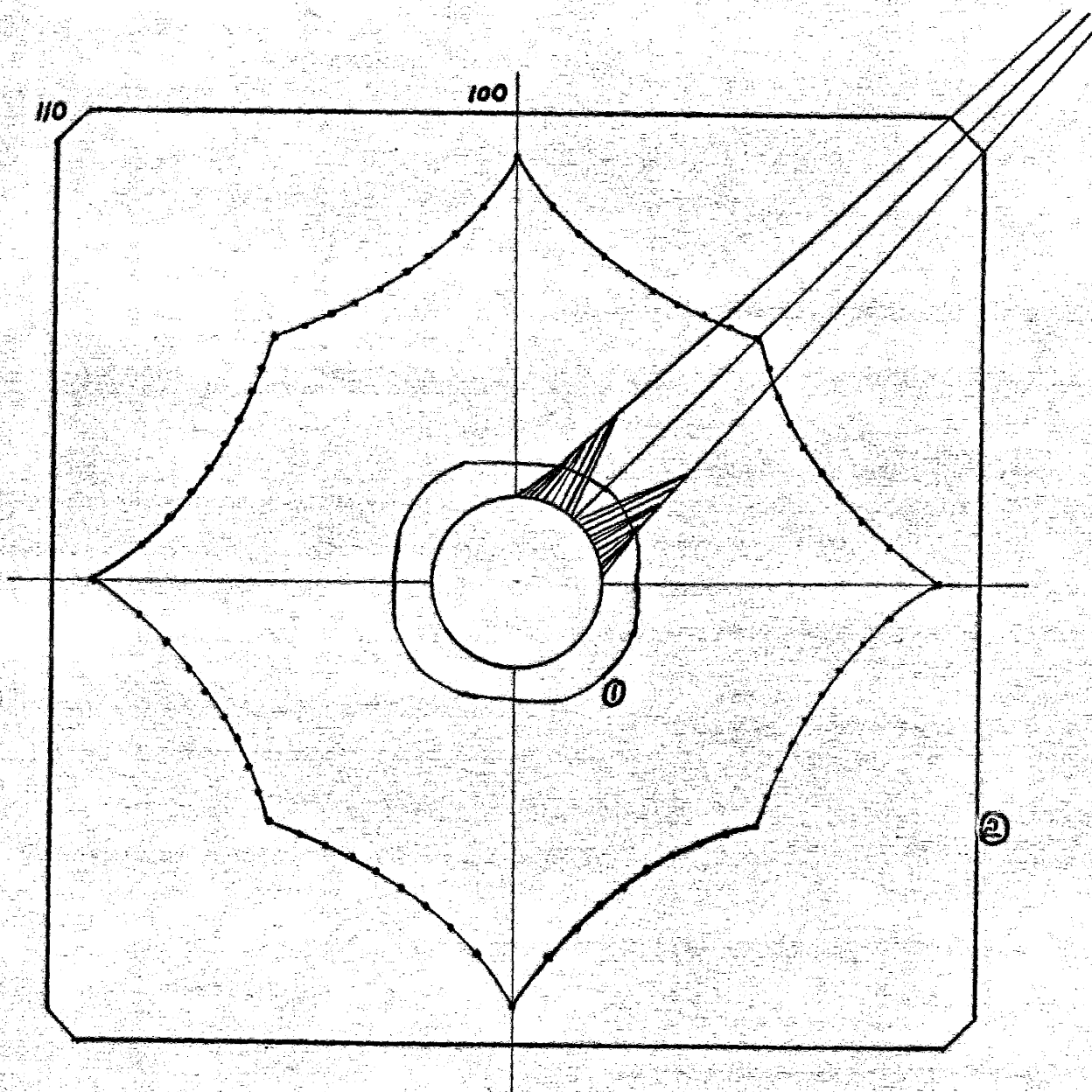
Fig. 27:   Reluctance diagram constructed from orientation dependent
etch rates obtained from fig. 24. Two predicted etch pit
shapes on a {100} surface are shown (1) corresponding to
an early time and (2) corresponding to a later time. For
clarity, only one quadrant of the diagram is shown in detail.
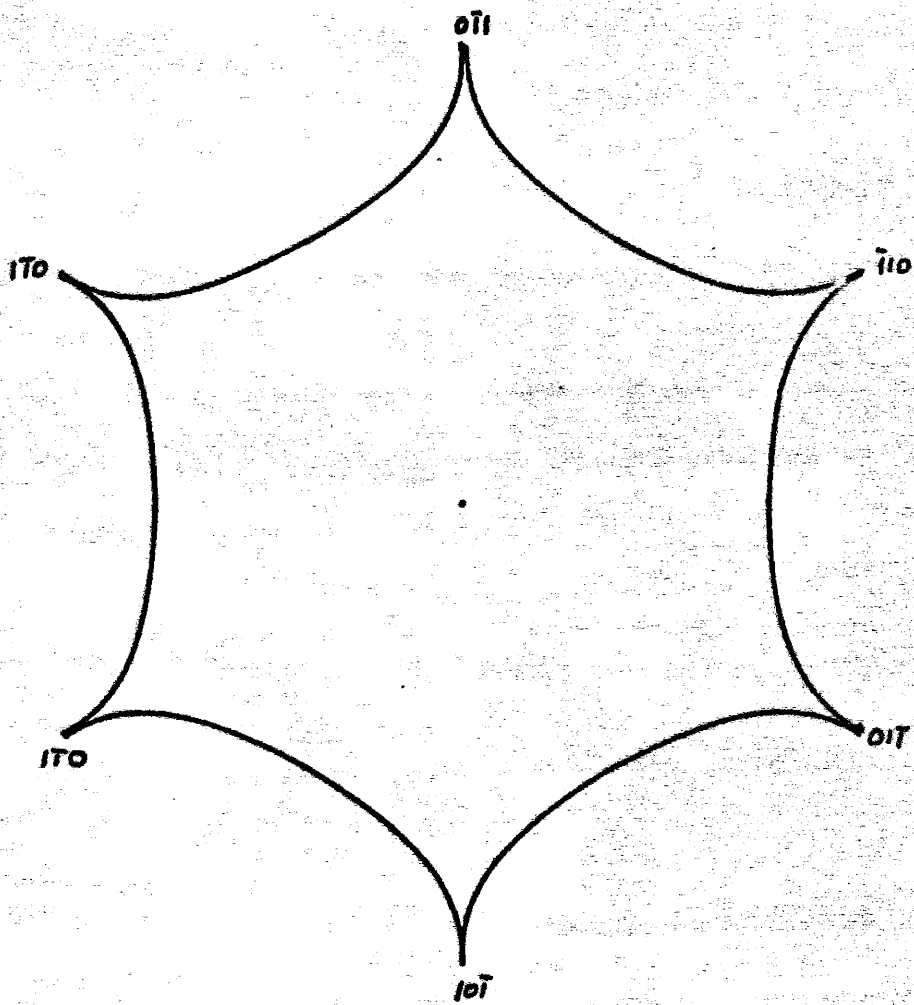
Fig. 28 :   Polar reluctance diagram constructed from etch rate data
            obtained from fig. 22.
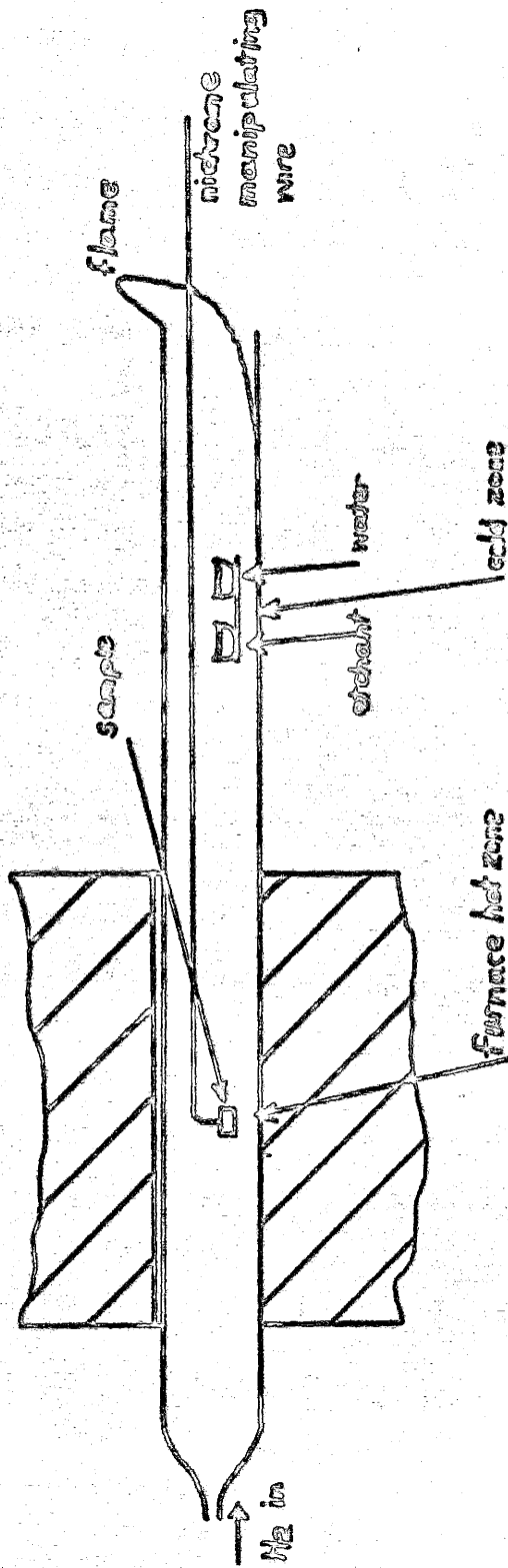
Fig. 29: Apparatus for preparing and etching oxide free iron surfaces.
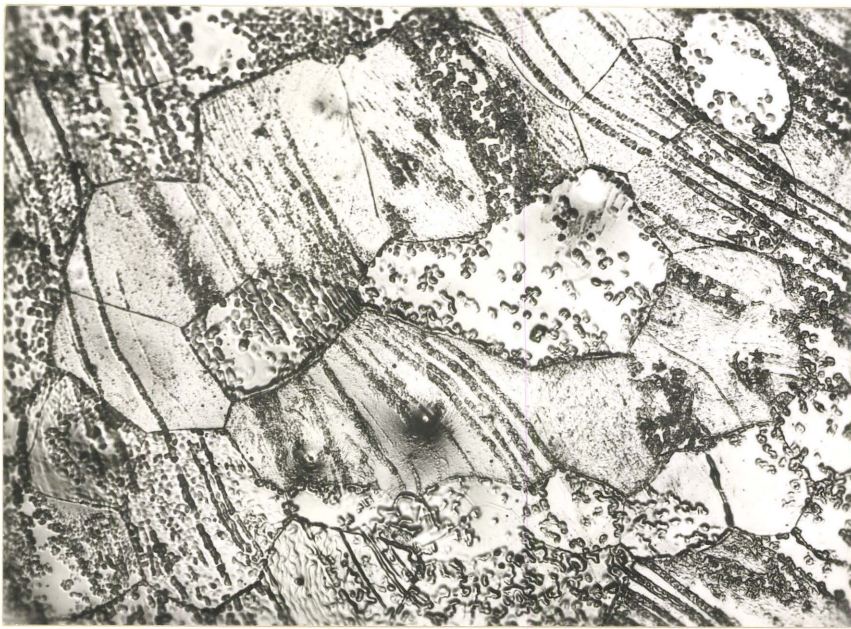
Fig. 30   Oxide free surface etched two seconds in Solution A X 200.
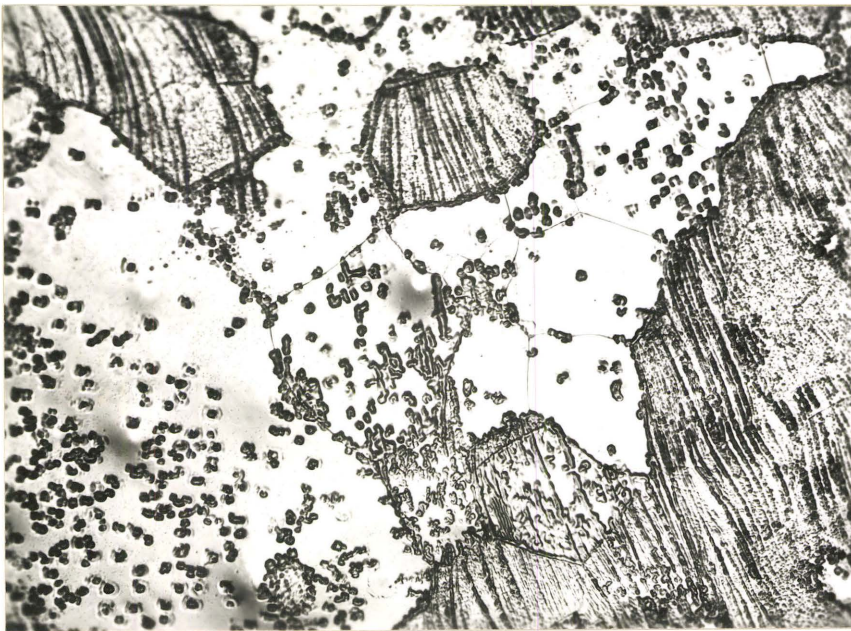
Fig. 31   As Fig. 30 X 200.
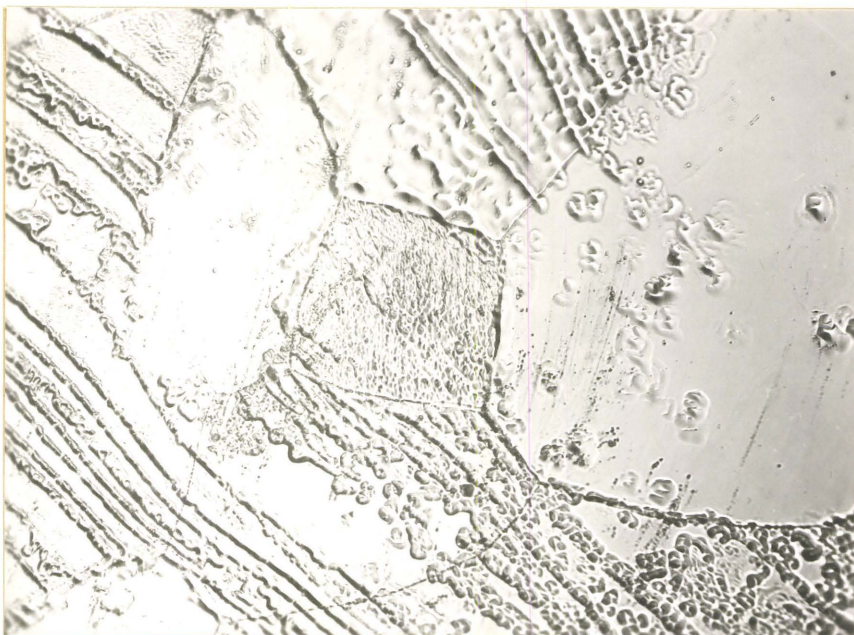
Fig. 32   As Fig. 30 X 500.

Fig. 33   Mechanically polished sample etched in hydrogen X 170.
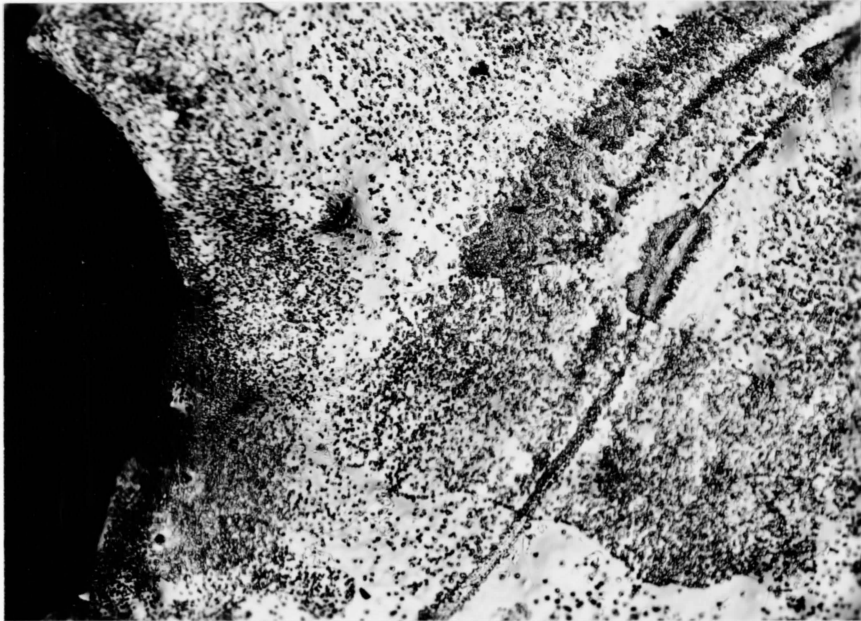
Fig. 34   Sample etched in hydrogen showing increased pit density
near hardness impression   X 68.
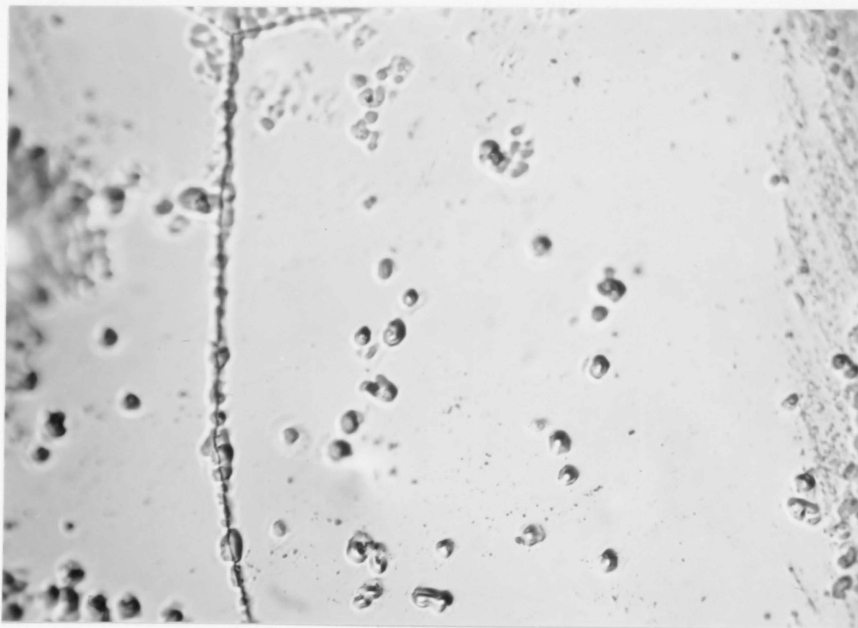
Fig. 35   Etched two seconds in A in hydrogen   X 500.
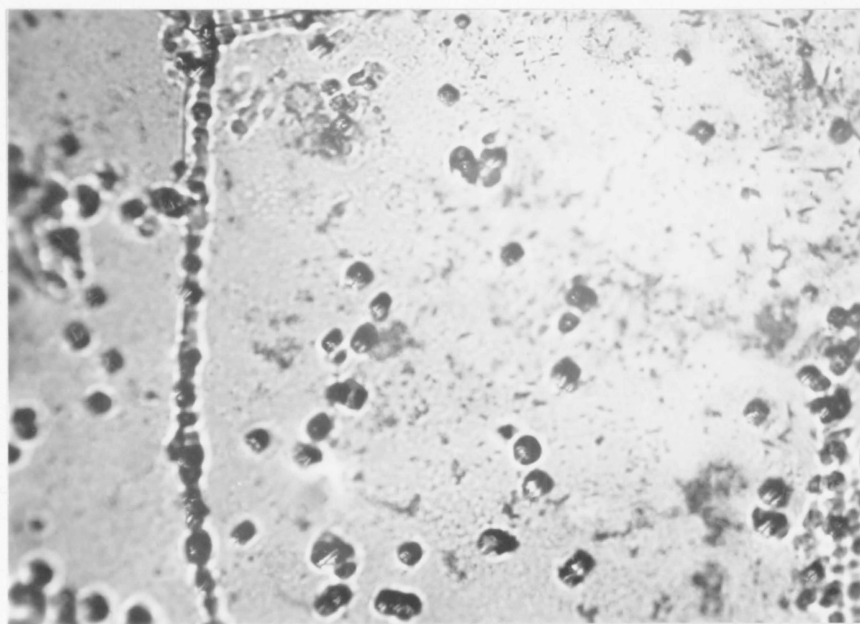
Fig. 36   Same field as Fig. 35 etched further two seconds in A in hydrogen X 500.

Fig. 37   Sample etched two seconds in A - undeformed   X 170.
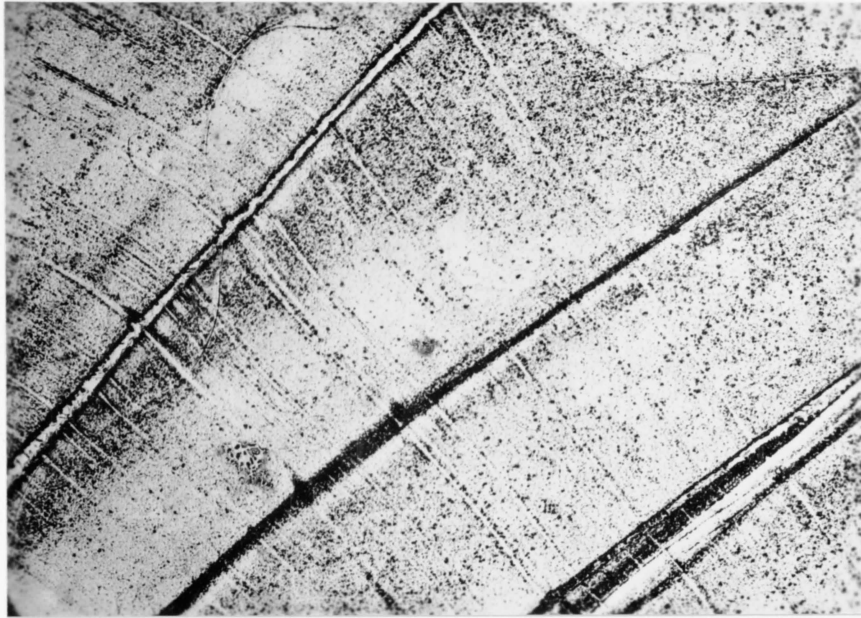
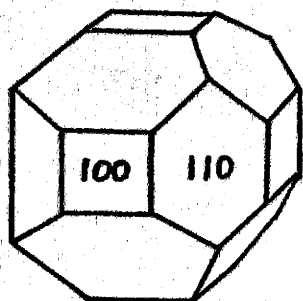Fig. 38   Mechanically polished sample showing slip bands after
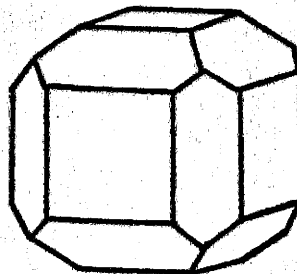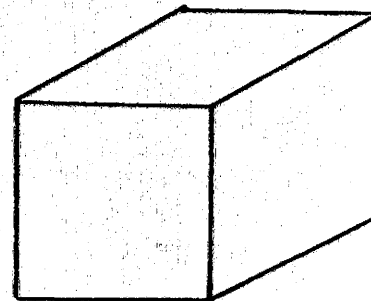etching in hydrogen X 68.
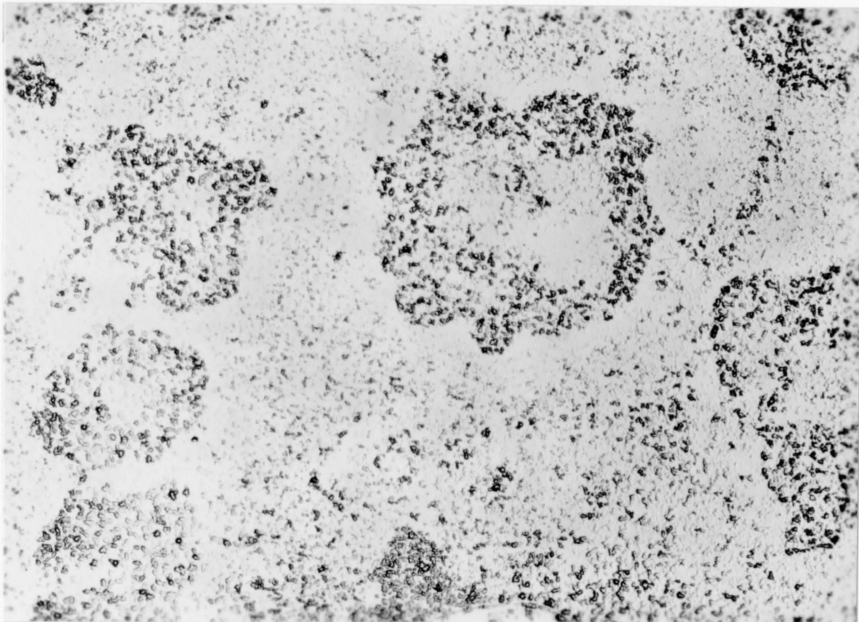
Fig. 39   As Fig. 38 X 170.

Fig. 40:   Shapes of pits derived from a hyperthetical 3-D reluctance
           surface.   (a) corresponding to profile (1) of fig. 27;
           (b) corresponding to profile (2) of fig. 27, and (c) the
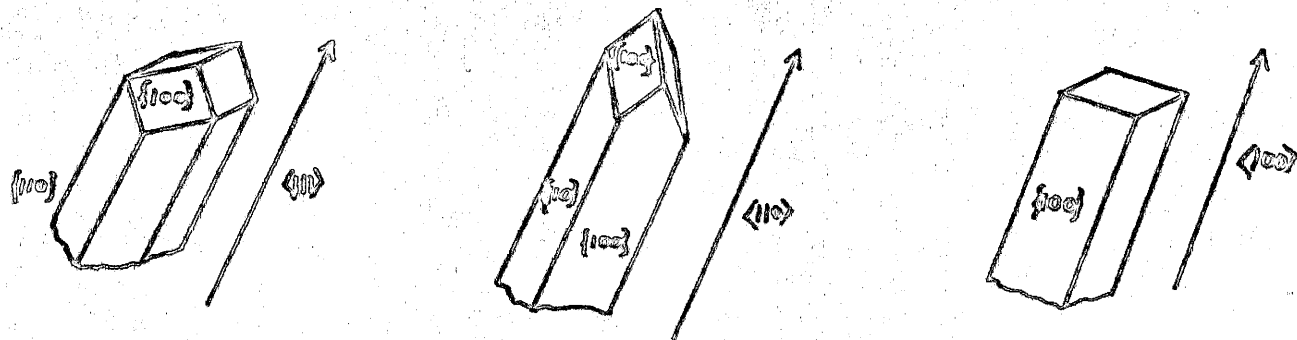   ultimate pit shape achieved after a long time in solution C.

Fig. 41 :   The three types of whiskers grown by the Brenner method.